36. B. Zipfel *et al.*, *Science* **333**, 1417 (2011).
37. R. J. Clarke, *S. Afr. J. Sci.* **95**, 477 (1999).
38. D. M. Alba, S. Moyà-Solà, M. Köhler, *J. Hum. Evol.* **44**, 225 (2003).
39. D. J. Green, A. D. Gordon, *J. Hum. Evol.* **54**, 705 (2008).
40. S. P. McPherron *et al.*, *Nature* **466**, 857 (2010).
41. M. W. Moore, T. Sutikna, Jatmiko, M. J. Morwood, A. Brumm, *J. Hum. Evol.* **57**, 503 (2009).

Acknowledgments: We thank the South African Heritage Resources Agency for the permits to work at the Malapa site; the Nash family for granting access to the Malapa site and continued support of research on the Malapa and John Nash nature reserves; the South African Department of Science and Technology, the South African National Research Foundation, the Institute for Human Evolution, University of the Witwatersrand, the University of the Witwatersrand's Vice Chancellor's Discretionary Fund, the National Geographic Society, the Palaeontological Scientific Trust, the Andrew W. Mellon Foundation, the Ford Foundation, the U.S. Diplomatic Mission to South Africa, the French embassy of South Africa, the Oppenheimer and Ackerman families, and Sir Richard Branson for funding; the University of the Witwatersrand's Schools of Geosciences and Anatomical Sciences and the Bernard Price Institute for Palaeontology for support and facilities; the Gauteng Government, Gauteng Department of Agriculture, Conservation and Environment and the Cradle of Humankind Management Authority; our respective universities for ongoing support; E. Mbua, P. Kiura, V. Iminjili, and the National Museums of Kenya, B. Billings, B. Zipfel, and the School of Anatomical Sciences at the University of the Witwatersrand, and S. Potze, L. C. Kgasi and the Ditsong Museum for access to comparative fossil specimens; the staff at the Musée royal de l'Afrique central, Museum für Naturkunde Berlin, Max-Planck-Institute für evolutionäre Anthropologie, Powell-Cotton Museum, Universität Wien, Naturhistorisches Museum Wien, Cleveland Museum of Natural History, Harvard Museum of Comparative Zoology, and Royal Ontario Museum for access to extant comparative material; and the University of Zurich 2010 Field School. Numerous individuals have been involved in the ongoing preparation and excavation of these fossils, including C. Dube, C. Kemp, M. Kgasi, M. Languza, J. Malaza, G. Mokoma, P. Mukanela, T. Nemvhundi, M. Ngcamphalala, S. Jirah, S. Tshabalala, and C. Yates. Other individuals who have given significant support to this project include B. de Klerk, W. Lawrence, C. Steininger, B. Kuhn, L. Pollarolo, J. Kretzen, D. Conforti, C. Dlamini, H. Visser, B. Nkosi, B. Louw, L. Backwell, F. Thackeray, and M. Peltier. J. Smilg facilitated computed tomography scanning of some of the specimens. We thank A. Deane for analysis of phalangeal curvature; and M. Skinner, D. Schmitt, D. Begun, and two anonymous reviewers for their constructive comments. This work was supported in part by the Natural Sciences Research Council of Canada and the Max Planck Society. Data are presented in the SOM.

Supporting Online Material
www.sciencemag.org/cgi/content/full/333/6048/1411/DC1
SOM Text S1 to S3
Figs. S1 to S18
Tables S1 to S13
References (*42*–*75*)

7 January 2011; accepted 29 July 2011
10.1126/science.1202625

The Foot and Ankle of *Australopithecus sediba*

Bernhard Zipfel,[1,2]* Jeremy M. DeSilva,[1,3] Robert S. Kidd,[1,4] Kristian J. Carlson,[1,5] Steven E. Churchill,[1,6] Lee R. Berger[1,7]

A well-preserved and articulated partial foot and ankle of *Australopithecus sediba*, including an associated complete adult distal tibia, talus, and calcaneus, have been discovered at the Malapa site, South Africa, and reported in direct association with the female paratype Malapa Hominin 2. These fossils reveal a mosaic of primitive and derived features that are distinct from those seen in other hominins. The ankle (talocrural) joint is mostly humanlike in form and inferred function, and there is some evidence for a humanlike arch and Achilles tendon. However, *Au. sediba* is apelike in possessing a more gracile calcaneal body and a more robust medial malleolus than expected. These observations suggest, if present models of foot function are correct, that *Au. sediba* may have practiced a unique form of bipedalism and some degree of arboreality. Given the combination of features in the *Au. sediba* foot, as well as comparisons between *Au. sediba* and older hominins, homoplasy is implied in the acquisition of bipedal adaptations in the hominin foot.

The human foot is thought to be one of the critical evolutionary specializations that define our species, being central to the evolution of arguably the most critical defining character of the Hominini: bipedalism (*1*–*5*). The increasing number of pedal elements in the hominin fossil record and the morphological diversity that they display have led some to conclude that there may have been greater diversity in early human bipedalism than previously thought (*6*). Foot and ankle elements of *Australopithecus sediba* shed light on the evolution of foot structure, giving a surprising look at a foot configuration with both primitive and derived characters that together have implications for our understanding of hominin bipedal diversity.

Well-preserved foot and ankle elements recovered from the Malapa site, South Africa (*7*, *8*), include an articulated distal tibia, talus, and calcaneus directly associated with the female paratype skeleton, Malapa Hominin 2 (MH2); two fragmentary metatarsals; and a calcaneal apophysis associated with the holotype juvenile male (MH1), as well as a distal tibia provisionally associated with MH1 (*7*) but now thought to probably originate from another individual (Fig. 1) (*9*).

Tibia, talus, and calcaneus. University of the Witwatersrand (U.W.) 88-97, 98, and 99 is the only associated complete adult partial (distal) tibia, talus, and calcaneus known in the early hominin fossil record (Fig. 2). The fossils were found in articulation and remain imprisoned in matrix (*7*). An attempt to physically separate the three elements in contact with one another would almost certainly result in damage to the specimens, risking destruction of delicate articular morphology (i.e., subchondral bone). Therefore, we sought an alternative preparation strategy: We used medical computed tomography (CT) to scan the specimen, removed the matrix digitally, and produced renderings of each element (*7*). Descriptions of U.W. 88-97, 98, and 99 are based on both the conjoined fossils and casts produced from high-resolution three-dimensional (3D) printouts of the digitally separated elements (Figs. 1A and 2) (*10*).

The U.W. 88-97 right tibia has an anteroposteriorly expanded metaphysis relative to the anteroposterior dimensions of the articular surface, a feature typical of bipedal hominins (fig. S1). In the coronal plane, the tibial plafond is perpendicular to the shaft, similar to that found in modern humans and fossil hominins (fig. S2), indirectly suggesting a valgus knee (*11*, *12*). In the sagittal plane, the posterior rim of the tibial plafond projects more inferiorly than the anterior rim, producing an anteriorly directed set of 6.7° to the ankle joint, suggesting arching of the foot (fig. S3) (*13*). The articular facet for the talus is slightly wedged in the inferior view and deeply curved in the lateral view, unlike the trapezoid-shaped and flat joint surface often found in apes (figs. S4 and S5). Discriminant function analysis clusters the MH2 tibia, as well as that originally associated with the MH1 skeleton, with humans and other fossil hominin tibiae [Fig. 3, supporting online material (SOM) text S1 and S2, and table S1]. However, both tibiae are dominated by an extremely robust medial malleolus, unlike the more gracile medial malleolus in modern humans and other fossil hominins, including *Au. africanus* (figs. S4 and S6).

U.W. 88-98 is a right talus with a humanlike moderately wedged trochlea. The trochlear body is ungrooved mediolaterally, similar to the condition in modern humans and some hominins such as A.L. 288-1 (*Au. afarensis*) and unlike many deeply grooved tali from other Plio-Pleistocene hominins such as that of OH 8 (*Homo habilis*)

[1]Institute for Human Evolution, University of the Witwatersrand, Post Office Wits, 2050 Wits, South Africa. [2]Bernard Price Institute for Palaeontological Research, School of Geosciences, University of the Witwatersrand, Post Office Wits, 2050 Wits, South Africa. [3]Department of Anthropology, Boston University, 232 Bay State Road, Boston, MA 02215, USA. [4]School of Biomedical and Health Sciences, University of Western Sydney, Cambelltown, New South Wales 2560, Australia. [5]Department of Anthropology, Indiana University, Bloomington, IN 47405, USA. [6]Department of Evolutionary Anthropology, Box 90383, Duke University, Durham, NC 27708, USA. [7]School of Geosciences, University of the Witwatersrand, Post Office Wits, 2050 Wits, South Africa.

*To whom correspondence should be addressed. E-mail: bernhard.zipfel@wits.ac.za

(fig. S7). The neck angle and head-torsion angle, however, appear to be apelike (table S2), whereas subequal trochlear heights on the medial and lateral sides are more reminiscent of the human form (fig. S7). The talar head is disproportionately large compared with the talar body, unlike those of humans and most fossil hominins, but within the range of those of apes (fig. S8). The talar neck and head have a strong plantar angle of inclination (fig. S9), suggestive of rear-foot arching (*14*), and the fibular facet does not face relatively superolaterally as is the case in many Plio-Pleistocene hominin tali, though this latter feature is highly variable in modern human tali (*15*). Morphometrically, the Malapa talus lies broadly between the African apes and humans (SOM text S1 and S3; fig. S10; and tables S3, S4, S5, and S6).

U.W. 88-99 is a right calcaneus and is the most complete *Australopithecus* example in the fossil record. As in human calcanei, the tuber is angled superodistally and possesses a smooth surface for the retrocalcaneal bursa underlying the Achilles tendon (*16*). There is also evidence for humanlike Sharpey's fibers (that is, bony fibers) at the enthesis for the Achilles tendon. The cuboid facet is angled plantarly, similar to the condition in modern humans and suggestive of an arched foot (*17*). Although postdepositional erosion precludes a definitive assessment of calcaneocuboid joint morphology, the portion that is preserved suggests a more mobile joint than that of modern humans. The peroneal trochlea is quite robust, suggesting a strong role for fibularis (peroneus) longus and brevis (*18*). Unlike the condition found in modern humans or in *Au. afarensis*, the lateral plantar process (LPP) is positioned superiorly with an apelike, near-horizontal orientation of the retrotrochlear eminence connecting the LPP and the peroneal trochlea (Fig. 4A and fig. S11). Where the weight-bearing LPP resides in calcanei of modern humans and *Au. afarensis*, there is instead a deep concavity in U.W. 88-99, most reminiscent of the feature expressed in the calcaneal body of gorillas. A strongly hollowed plantar surface creating a beaklike morphology to the medial plantar process is also apelike and may imply an important role for the superficial head of the flexor digitorum brevis (*19*), abductor hallucis, and even abductor digiti minimi/quinti.

The calcaneal tuber is gracile, representing a cross-sectional area of 3.53 cm^2, which is about half the value calculated from modern humans and *Au. afarensis* (*20*). The minimum tuber volume is 13.44 cm^3, similar to the condition found in chimpanzees and female gorillas and distinct from that found in modern humans and other early hominins (table S7). If we treat tuber volume as a fraction of body mass (~26 to 35 kg), the *Au. sediba* calcaneus is 0.38 to 0.52 cm^3/kg, which is higher than the value found in modern African apes (0.20 to 0.25 cm^3/kg) but smaller than the value found in modern humans (0.70 to 0.78 cm^3/kg) (table S7). Relative to the long axis

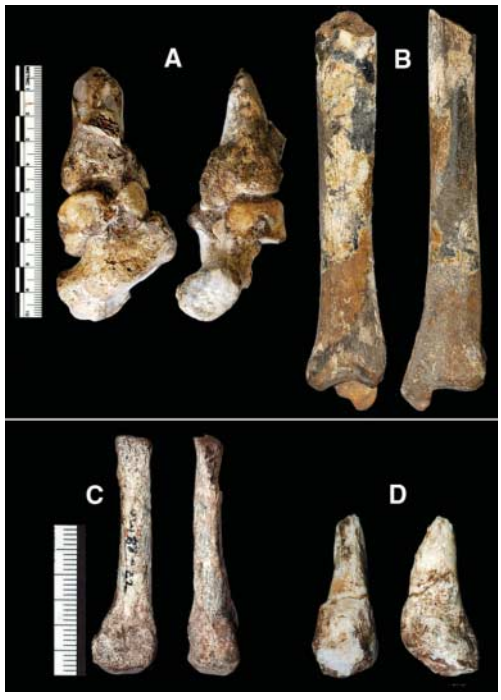

Fig. 1. Partial foot and leg elements of *Au. sediba*. (**A**) U.W. 88-97, 98, and 99 right distal tibia, talus, and calcaneus (MH2) in a near anatomical relationship, cemented together with calcified sediment. Lateral view, left; posterior view, right. (**B**) U.W. 88-21 right distal tibia. Lateral view, left; posterior view, right. (**C**) U.W. 88-22 right fourth metatarsal. Medial view, left; dorsal view, right. (**D**) U.W. 88-33 right proximal fifth metatarsal. Medial view, left; dorsal view, right. A calcaneal apophysis (not illustrated in this figure; see Fig. 4A) was recently discovered and appears to be associated with MH1.

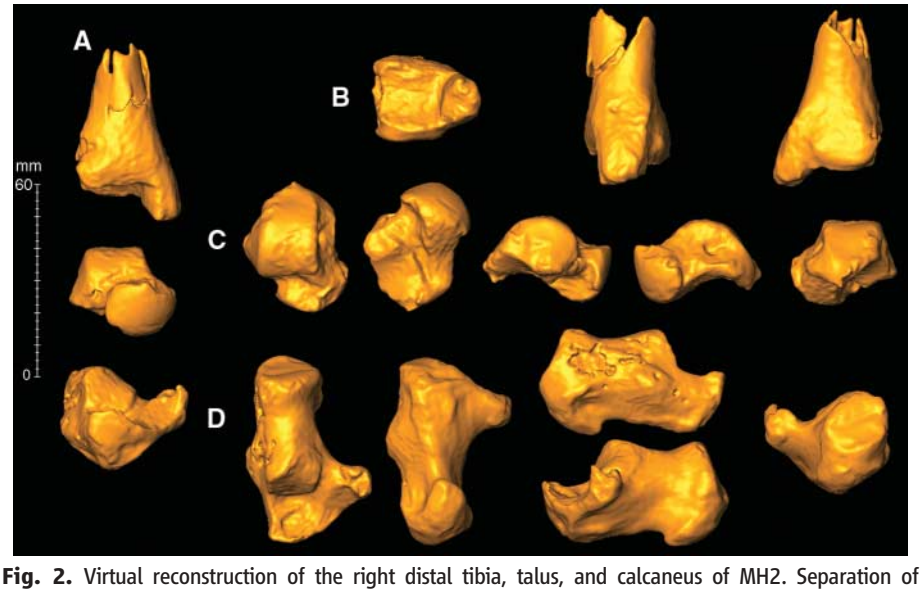

Fig. 2. Virtual reconstruction of the right distal tibia, talus, and calcaneus of MH2. Separation of elements: (**A**) Distal tibia, top; talus, middle; calcaneus, bottom. All anterior views. (**B**) Tibia views from left to right: inferior, medial, posterior. (**C**) Talus views from left to right: superior, inferior, lateral, medial, posterior. (**D**) Calcaneus views from left to right: superior, inferior, lateral (top), medial (bottom), posterior.

Fig. 3. Discriminant function analysis of the tibiae U.W. 88-21 and U.W. 88-97. These analyses were carried out using 11 measurements of the distal tibia (SOM text S2 and table S1). Function one is being driven in part by the anterior width of the tibial plafond and thickness of the medial malleolus (greater dimensions to right), as well as the anteroposterior expansion of the metaphysis (to the left). The Malapa hominins cluster with humans, australopiths, and fossil *Homo*.

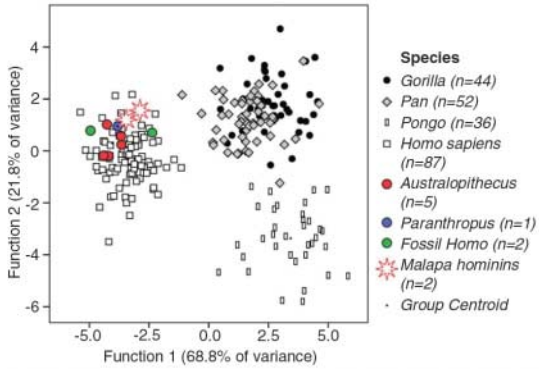

of the bone, the tuber is also medially deviated 13°, which would promote foot inversion with plantarflexion during activation of the triceps surae. The talar facet is strongly convex, with a subtended angle similar to the mobile subtalar joint found in chimpanzees and gorillas, but is quite distinct from the flat joint surface of modern humans and fossil hominins (table S7). Plantarly, there is a rugosity for attachment of the long plantar ligament, an important stabilizer of the midfoot in humans (fig. S12). Canonical variates analysis suggests that the U.W. 88-99 calcaneal body is decidedly similar to that of an African ape (Fig. 4B; SOM text S1 and S3; fig. S13; and tables S5, S6, S8, and S9).

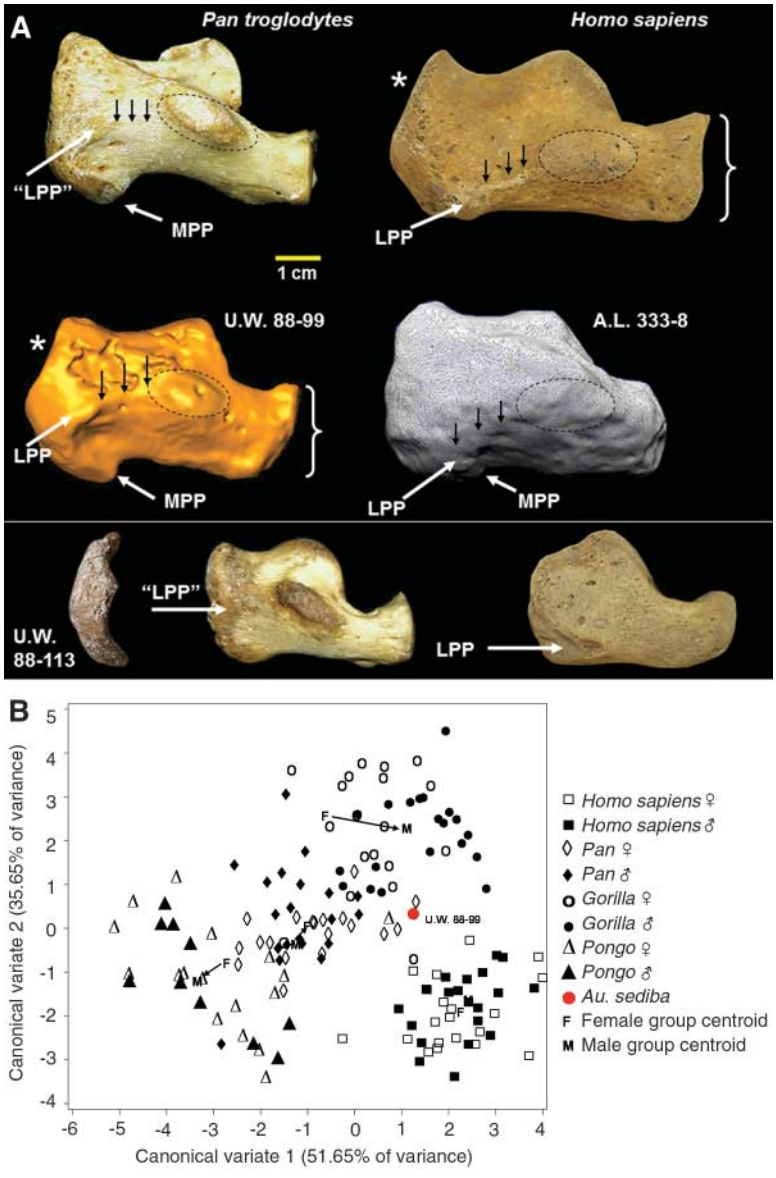

Fig. 4. (**A**) Right calcanei illustrating the salient features discussed in the text. The peroneal trochlea is indicated with a dashed circle; black arrows point toward the retrotrochlear eminence connecting the peroneal trochlea and the LPP. MPP, medial plantar process. As demonstrated elsewhere (*20*), humans have an obliquely oriented retrotrochlear eminence and a plantarly positioned LPP, such that in lateral view, the MPP is often not visible at all. This general pattern is also found in *Au. afarensis* (A.L. 333-8) and is present already in juvenile humans (bottom right). In contrast, *Au. sediba* (U.W. 88-99) possesses a more apelike orientation of the retrotrochlear eminence and a superiorly positioned, non–weight-bearing LPP such that the MPP is clearly visible in lateral view. An elevated structure homologous to the LPP can be found in both adult and juvenile apes (bottom left) and is visible in the juvenile *Au. sediba* apophysis (U.W. 88-113 reversed image). However, *Au. sediba* has a humanlike angled cuboid facet (denoted by brackets), which is suggestive of foot arching, and a flat, smooth surface of the calcaneal tuber, perhaps for a retrocalcaneal bursa underlying an elongated Achilles tendon (asterisks). (**B**) Canonical variates analysis of the calcaneus using eight indices (SOM text S3 and tables S4 and S6). The plot of canonical means along canonical variates 1 and 2 (great apes, humans, and fossil) shows a discrimination of U.W. 88-99 between humans and African apes but shows the greatest affinity to female African apes. *Homo*, *Pan*, and *Gorilla* (n = 20 males, 20 females) and *Pongo* (n = 10 males, 17 females) are represented here.

Tibia. U.W. 88-21 is an isolated right distal tibia and partially conjoining fragment of the proximal diaphysis. The shaft is straight and does not exhibit the anterior and lateral bowing of the tibial shaft found in African apes. The distal tibia is anatomically and morphometrically similar to that of U.W. 88-97 (Figs. 1B and 3, fig. S4, and table S1).

Metatarsals. U.W. 88-22 is a right juvenile fourth metatarsal. What is preserved of the proximal articular surface appears convex dorsoplantarly (Fig. 1C). U.W. 88-33 is a right proximal fifth metatarsal, estimated to represent a little less than half of the total length of the bone. The shaft curves in the transverse plane with the concavity on the lateral side, and the base is expanded as in humans and extinct hominins (Fig. 1D). Both the proximal and medial articular surfaces are weakly convex dorsoplantarly, similar to those of humans and extinct hominins (*21*).

Calcaneal apophysis. U.W. 88-113 is a left apophysis most likely associated with MH1. Its morphology is similar to that of U.W. 88-99 (Fig. 4A).

Functional interpretation. The foot and ankle of *Au. sediba* reveal a mosaic of primitive and derived features of the hominin foot unlike any combination known in the human fossil record. The ankle (talocrural joint) represented by the associated fossils U.W. 88-97 and U.W. 88-98, as well as U.W. 88-21, is mostly humanlike. The *Au. sediba* fossils possess a distribution of bone around the tibial articular surface that is humanlike in being expanded posteriorly and laterally. The tibial plafond is deep and the metaphysis is anteroposteriorly expanded, both adaptations for bipedality found in human and fossil hominin distal tibiae. Perhaps most critical from a functional standpoint, the distal tibial articular surface is orthogonal to the long axis of the shaft in the coronal plane, a morphology that positions the knee over the foot and may be indirectly related to the presence of a valgus knee (*11*, *12*). Though skeletal correlates of an arched foot are not entirely agreed on, angulation of the tarsal joints suggests that *Au. sediba* had an arched foot. Furthermore, the angled calcaneal tuber, Sharpey's fibers, and flat surface for a bursa suggest that *Au. sediba* may have possessed a humanlike tendinous insertion for the triceps surae, though Achilles tendon length is not obvious from external calcaneal morphology alone (*22*, *23*). Considering this suite of derived characters, the primitive apelike calcaneal body and medial malleolus are unexpected.

The *Au. sediba* foot is primitive in force transmission through the heel and subtalar joint. The calcaneus is gracile, having a size-standardized volume outside the lower range estimated for *Au. afarensis* calcanei (table S7). It also differs considerably from the calcanei of *Au. afarensis* in positioning of the LPP. As detailed by Latimer and Lovejoy (*20*), both modern human and *Au. afarensis* calcanei differ from those of the

African apes in having a plantarly positioned LPP connected to the peroneal trochlea via an obliquely oriented retrotrochlear eminence. African apes, in contrast, possess a more horizontally oriented retrotrochlear eminence, terminating in a bony flange homologous to the LPP. Although the position of the LPP alone may not be adaptive and may simply be a by-product of calcaneal tuber expansion in bipedal hominins, it is notable that the contrasting positions of the LPP are already expressed in juvenile humans and apes. The latter observation makes recent recovery of an apelike calcaneal aphophysis from MH1 important (Fig. 4A). Given the many derived features of the *Au. sediba* foot, pelvis (*24*), hand (*25*), and craniodental anatomy (*7*), it is curious that the LPP position is apelike. This primitive morphology suggests (if *Au. sediba* is more closely related to *Homo* than is *Au. afarensis*) that reorganization of the calcaneal body may have evolved convergently in modern humans and earlier hominins. Alternatively (if *Au. afarensis* is more closely related to *Homo* than is *Au. sediba*), derived features in the *Au. sediba* skeleton not found in *Au. afarensis* would have had to have evolved independently in *Au. sediba* and in the human lineage. Regardless, the *Au. sediba* fossils suggest that foot evolution during the Plio-Pleistocene may have been complex, involving mosaic acquisition of modern anatomies in multiple hominin lineages or even evolutionary reversals. The absence of a weight-bearing LPP has functional relevance as well. Terrestrial apes have a beaklike medial plantar process that contacts the ground during heel-strike (*26*). However, quadrupedal apes can distribute their body mass across multiple contact points (limbs), reducing the load on any one limb throughout the gait cycle. *Au. sediba* is clearly bipedal, but because the LPP is not in a weight-bearing position, the ground reaction force produced at heel-strike would be concentrated on the medial plantar process, producing elevated stress on the heel. How *Au. sediba* modified gait behavior kinematically to alter this kinetic implication remains unclear.

In addition to the apelike plantar processes, there is evidence for considerable mobility at the subtalar joint that would allow more inversion than is possible in the modern human foot. Consistent with this anatomy are medial malleoli of the two distal tibiae from Malapa that are markedly thick, beyond the range in both modern humans and other fossil hominins. Unlike climbing cercopithecoids, great apes load the medial aspect of their foot and ankle during vertical climbing bouts (*27*). A functional correlate of inverted/dorsiflexed foot vertical climbing may be a robust medial malleolus, which is present in climbing hominoids and atelines but is substantially more gracile in cercopithecoids and hominins (*28*). The robust medial malleolus in both *Au. sediba* tibiae may therefore indicate some degree of climbing. The absence of a mediolaterally expanded anterior rim of the distal tibial articular surface indicates that *Au. sediba* may not have been climbing with as highly dorsiflexed an ankle as in modern apes (*12*) but instead could have been loading an inverted foot during humanlike pulse climbing bouts. Taken together with the highly mobile subtalar joint, these features suggest that exploitation of arboreal habitats was an important part of the behavioral ecology of *Au. sediba*.

At ~1.98 million years ago (*29*), the combination of morphologies in the *Au. sediba* foot is different from that found in the foot of the older *Au. afarensis*, which has a more derived calcaneal corpus and humanlike medial malleolus but less obvious evidence for a long tendon of triceps surae. These contrasts support the notion that the acquisition of bipedal adaptations in the hominin lineage evolved in a mosaic fashion and is more complex than previously thought. The constellation of primitive and derived features in the foot skeleton of both *Au. afarensis* and *Au. sediba* raises these intriguing possibilities: (i) An ancestor-descendant relationship (either directly or via an intermediate species such as *Au. africanus*) between these two species is unlikely, indicating a more distant common ancestor, or (ii) if such a relationship did exist, it would require evolutionary reversals in calcaneal and distal tibial morphology, despite habitual bipedal locomotion in both species.

References and Notes

1. O. J. Lewis, *J. Anat.* **131**, 275 (1980).
2. D. J. Morton, *The Human Foot: Its Evolution, Physiology, and Functional Disorders* (Columbia Univ. Press, New York, 1935).
3. F. W. Wood Jones, *Structure and Function as Seen in the Foot* (Bailliere, Tindall and Cox, London, 1944).
4. M. H. Day, J. R. Napier, *Nature* **201**, 969 (1964).
5. R. L. Susman, *Foot Ankle* **3**, 365 (1983).
6. W. E. Harcourt-Smith, L. C. Aiello, *J. Anat.* **204**, 403 (2004).
7. L. R. Berger *et al.*, *Science* **328**, 195 (2010).
8. P. H. G. M. Dirks *et al.*, *Science* **328**, 205 (2010).
9. The absence of an epiphyseal line in the U.W. 88-21 right distal tibia suggests that it is not from a juvenile and therefore is unlikely to be from MH1. The remainder of the MH1 skeleton's dental and epiphyseal development is consistent with the age originally described (*7*). This tibia also does not belong to MH2, as the right tibia U.W. 88-97 (bound by matrix to the talus and calcaneus) is clearly directly associated with this individual.
10. Most of the comparative linear dimensions used in this study were collected on the original fossils using digital sliding calipers. To maximize measurement comparability and justify performing statistical analyses when pooling these data and data from the Malapa fossils, a high-resolution 3D printer was employed to produce 1:1 powder-based printouts from the renderings. The printouts were subsequently cast for distribution. Casts were validated by comparing measurements taken from exposed features of the original fossils with measurements taken from homologous features on the casts; differences were <0.5 mm. Measurements were taken on the casts following the same protocol as was applied when collecting the comparative data.
11. B. Latimer, J. C. Ohman, C. O. Lovejoy, *Am. J. Phys. Anthropol.* **74**, 155 (1987).
12. J. M. DeSilva, *Proc. Natl. Acad. Sci. U.S.A.* **106**, 6567 (2009).
13. J. M. DeSilva, Z. J. Throckmorton, *PLoS ONE* **5**, e14432 (2010).
14. M. H. Day, B. A. Wood, *Man (London)* **3**, 440 (1968).
15. C. O. Lovejoy, in *Early Hominids of Africa*, C. E. Jolly, Ed. (Duckworth, London, 1978), pp. 403–429.
16. D. Kachlik *et al.*, *Surg. Radiol. Anat.* **30**, 347 (2008).
17. G. Berillon, *Hum. Evol.* **18**, 113 (2003).
18. J. T. Stern Jr., R. L. Susman, *Am. J. Phys. Anthropol.* **60**, 279 (1983).
19. E. E. Sarmiento, *Int. J. Primatol.* **4**, 127 (1983).
20. B. Latimer, C. O. Lovejoy, *Am. J. Phys. Anthropol.* **78**, 369 (1989).
21. B. Zipfel, J. M. DeSilva, R. S. Kidd, *Am. J. Phys. Anthropol.* **140**, 532 (2009).
22. W. I. Sellers, T. C. Pataky, P. C. Caravaggi, R. H. Crompton, *Int. J. Primatol.* **31**, 321 (2010).
23. All of the human calcanei that we studied possess this combination of an angled calcaneal tuber, Sharpey's fibers, and a flat surface for a bursa. No chimpanzees (n = 24) possessed these features together. However, these three features were found in a small number of gorilla calcanei (n = 5 out of 25).
24. J. M. Kibii *et al.*, *Science* **333**, 1407 (2011).
25. T. L. Kivell, J. M. Kibii, S. E. Churchill, P. Schmid, L. R. Berger, *Science* **333**, 1411 (2011).
26. D. L. Gebo, *Am. J. Phys. Anthropol.* **89**, 29 (1992).
27. R. E. Wunderlich, thesis, State University of New York, Stony Brook (1999).
28. J. M. DeSilva, thesis, University of Michigan (2008).
29. R. Pickering *et al.*, *Science* **333**, 1421 (2011).

Acknowledgments: We thank the South African Heritage Resources agency for the permits to work at the Malapa site; the Nash family for granting access to the Malapa site and continued support of research on the Malapa and John Nash nature reserves; the South African Department of Science and Technology, the South African National Research Foundation, the Institute for Human Evolution, Univ. of the Witwatersrand, Univ. of the Witwatersrand's Vice Chancellor's Discretionary Fund, the National Geographic Society, the Palaeontological Scientific Trust, the Andrew W. Mellon Foundation, the Ford Foundation, the U.S. Diplomatic Mission to South Africa, the French Embassy of South Africa, the Leakey Foundation, the Oppenheimer and Ackerman families, and R. Branson for funding; the Univ. of the Witwatersrand's Schools of Geosciences and Anatomical Sciences and the Bernard Price Institute for Palaeontological Research for support and facilities; the Gauteng Government, Gauteng Department of Agriculture, Conservation and Environment and the Cradle of Humankind Management Authority; and our respective universities for ongoing support. We also thank S. Potze, L. Kgasi and the Ditsong Museum of Natural History (Pretoria), E. Mbua, P. Kiura, V. Iminjili and the National Museums of Kenya, A. Kwekason, P. Msemwa and the Tanzania Commission for Science and Technology and B. Billings and the Univ. of the Witwatersrand fossil access advisory panel for access to comparative specimens; Y. Haile-Selassie, L. Jellema and the Cleveland Museum of Natural History, J. Chupasko and the Harvard Museum of Comparative Zoology, D. Pilbeam, M. Morgan and the Harvard Peabody Museum, O. Lovejoy, D. Gebo, M. Wolpoff, and staff of the Smithsonian Institution, American Museum of Natural History, Chicago Field Museum, Powell-Cotton Museum, and The Natural History Museum (London) for access to comparative fossil casts, as well as human and ape skeletal specimens. Additionally, we are grateful to the Univ. of Zurich 2010 Field School. Numerous individuals have been involved in the ongoing preparation and excavation of these fossils, including C. Dube, C. Kemp, M. Kgasi, M. Languza, J. Malaza, G. Mokoma, P. Mukanela, T. Nemvhundi, M. Ngcamphalala, S. Jirah, S. Tshabalala, and C. Yates. Other individuals who have given considerable support to this project include B. de Klerk, W. Lawrence, C. Steininger, B. Kuhn, L. Pollarolo, J. Kretzen, D. Conforti, C. Dlamini, H. Visser, B. Nkosi, B. Louw, L. Backwell, F. Thackeray, M. Peltier, J. McCaffery, and R. McCrae-Samuel. J. Smilg facilitated CT scanning of the specimens. Finally, we thank G. Leggott, D. Bullock, and P. Bullock from Rapid3D-produced 3D printouts and R. Wunderlich, C. Ward, T. Kivell, B. Hanson, and four anonymous reviewers for helpful comments.

Supporting Online Material

www.sciencemag.org/cgi/content/full/333/6048/1417/DC1
Materials and Methods
SOM Text
Figs. S1 to S14
Tables S1 to S9
References (*30*–*51*)

10 January 2011; accepted 29 July 2011
10.1126/science.1202703

Supporting Online Material for

The Foot and Ankle of *Australopithecus sediba*

Bernhard Zipfel,* Jeremy M. DeSilva, Robert S. Kidd, Kristian J. Carlson, Steven E. Churchill, Lee R. Berger

*To whom correspondence should be addressed. E-mail: bernhard.zipfel@wits.ac.za

Published 9 September 2011, *Science* **333**, 1417 (2011)
DOI: 10.1126/science.1202703

This PDF file includes:

SOM Text S1 to S3
Tables S1 to S9
Figures S1 to S14

TEXT S1. Materials

The tibiae and tali of non-human hominoids used in the univariate and discriminant functions analysis were all wild-collected adults from the Cleveland Museum of Natural History, Field Museum (Chicago), American Museum of Natural History, Harvard Museum of Comparative Zoology, and the National Museum of Natural History (Smithsonian). The human tibiae were from the 9^{th}-12^{th} century PaleoIndian Libben population housed at Kent State University, the Hamann-Todd collection at the Cleveland Museum of Natural History, and an unprovenienced sample of human tibiae from the University of Michigan Department of Anthropology. These are listed below:

Extant tibiae measured in this study for the univariate and Discriminant Function Analysis.

Species	**Male**	**Female**	**Sex unknown**	**Total**
Homo sapiens	25	34	86	145
Pan troglodytes	18	20	11	49
Pan paniscus	2	1	1	4
Gorilla gorilla	23	19	7	49
Pongo pygmaeus	12	19	5	36

Extant tali measured in this study for the univariate analysis presented in Fig. S8.

Species	**Male**	**Female**	**Sex unknown**	**Total**
Homo sapiens	13	21	46	80
Pan troglodytes	17	20	9	46
Gorilla gorilla	23	19	2	44

Associated calcanei and tali of non-human hominoids used in the canonical variates analysis were all wild-collected adults from the National Museum of Natural History (Smithsonian) and Powell-Cotton Museum. The human calcanei and tali were from Victorian British (Spitalfields Collection) from the Natural History Museum (London). These are listed below:

Extant associated tali and calcanei measured for the canonical variates analysis.

Species	Male	Female	Total
Homo sapiens	20	20	40
Pan troglodytes	20	20	40
Pan paniscus	20	20	40
Gorilla gorilla	20	20	40
Pongo pygmaeus	10	17	27

The hominin fossil tali and tibiae used in this study were from the University of the Witwatersrand, Johannesburg; Ditsong Museum of Natural History, Pretoria, the Kenya National Museum, Nairobi; National Museum and House of Culture, Dar Es Salaam; and high quality casts of *Au. afarensis* at the Harvard Peabody Museum, and Cleveland Museum of Natural History. These are listed below:

Fossil tali and tibiae measured in this study.

Accession number	Element	Geological age (m.a.) (reference)	Species designation
KNM-KP 29285	Tibia	4.12 *(30)*	*Australopithecus anamensis*
A.L. 333-6	Tibia	3.2 *(31)*	*Au. afarensis*
A.L. 333-7	Tibia	3.2 *(31)*	*Au. afarensis*
A.L. 333-8	Calcaneus	3.2 *(31)*	*Au. afarensis*
A.L. 333-55	Calcaneus	3.2 *(31)*	*Au. afarensis*
A.L. 288-1	Talus	3.18 *(31)*	*Au. afarensis*
A.L. 288-1	Tibia	3.18 *(31)*	*Au. afarensis*
StW 181	Tibia	2.0-2.6 *(32)*	*Au. africanus*
StW 347	Talus	2.0-2.6 *(32)*	*Au. africanus*
StW 358	Tibia	2.0-2.6 *(32)*	*Au. africanus*
StW 363	Talus	2.0-2.6 *(32)*	*Au. africanus*
StW 389	Tibia	2.0-2.6 *(32)*	*Au. africanus*
StW 88	Talus	2.0-2.6 *(32)*	*Au. africanus*
StW 514b	Tibia	2.0-2.6 *(32)*	*Au. africanus*
StW 486	Talus	2.0-2.6 *(32)*	*Au. africanus*
StW 102	Talus	2.0-2.6 *(32)*	*Au. africanus*
StW 352	Calcaneus	2.0-2.6 *(32)*	*Au. africanus*
Omo 33-74-896	Calcaneus	2.36 *(33)*	Hominid *Homo*?
Omo 323-76-898	Talus	2.2 *(33)*	Hominid *Homo*?
TM 1517	Talus	1.4-1.8 *(34)*	*Paranthropus robustus*
SKX 42695	Talus	1.4-1.8 *(34)*	*P. robustus? Homo?*
KNM-ER 1481	Tibia	1.9 *(34)*	*H. habilis?*

			H. erectus
KNM-ER 1500	Tibia	1.9 *(33)*	*P. boisei?*
KNM-ER 2596	Tibia	1.9 *(33)*	Hominid
KNM-ER 1476	Talus	1.88 *(33)*	*P. boisei?*
OH 8	Talus	1.8 *(35)*	*H. habilis?*
			P. boisei?
OH 35	Tibia	1.8 *(35)*	*H. habilis?*
			P. boisei?
KNM-ER 813	Talus	1.85 *(33)*	*Homo?*
KNM-ER 1464	Talus	1.7 *(33)*	*P. boisei?*
			Homo?
StW 567	Tibia	1.4-1.7 *(32)*	*Homo?*
KNM-ER 5428	Talus	1.6 *(33)*	*H. erectus*
KNM-WT 15000	Tibia	1.5 *(36)*	*H. erectus*

TEXT S2. Discriminant function analysis of tibiae

Six measurements were taken on the articular surface of the distal tibia. These are illustrated in SOM Fig. S14:
1.) The maximum mediolateral length of the anterior aspect of the articular surface.
2.) The maximum mediolateral length of the posterior aspect of the articular surface.
3.) The maximum mediolateral length at the midpoint of the articular surface.
4.) The maximum anteroposterior width of the most medial aspect of the articular surface.
5.) The maximum anterioposterior width of the most lateral aspect of the articular surface.
6.) The maximum anteroposterior width at the midpoint of the articular surface.

Three measurements were taken on the medial malleolus:
1.) The maximum mediolateral thickness.
2.) The maximum anteroposterior length of the malleolus taken perpendicular to the medial malleolar width.
3.) The malleolar height taken as the maximum superoinferior projection of the malleolus from the articular surface.

Two measurements of the metaphysis were taken:
1.) The mediolateral width of the tibial metaphysis was taken as the maximum mediolateral dimension at the point where the medial malleolus begins to curve medially, just superior to the distal articular surface. The medial malleolus itself, however, was not included in the measurement.
2.) The anteroposterior dimension was the maximum width perpendicular to the mediolateral dimension.

The geometric mean of these 11 measures was calculated by taking the product and then the (1/11)th root of the product. Each raw measurement was then divided by the geometric mean, and entered into a non-stepwise discriminant function analysis using SPSS 16.0. All of the fossils were entered as separate groups.

TEXT S3 Canonical variates analysis of the talus and calcaneus

Justification of reference planes and dimensions.

All reference planes and dimensions used in this study have been defined previously (37), and used extensively elsewhere, in whole or in part (38-*42*).

Talar Dimensions:

1) The maximum medial height is the projected height from the standard basal talar plane to the highest point on the medial margin of the trochlear facet.

2) The maximum lateral height is the projected height from the standard talar basal plane to the highest point on the lateral margin of the trochlear facet.

3) The maximum median height of the talus is the projected height from the talar basal plane to highest point on the median trochlear arc.

The above three measurements were obtained by resting the talus upon a glass plate of known thickness, the measurement being from the underneath surface of the glass to the required maximum height. The thickness of the glass was included in the raw data collection to avoid confusion and subsequently subtracted.

4) The transverse trochlear breadth is the distance between the medial and lateral margins of the trochlear facet taken in the coronal talar plane.

5) The anterior trochlear breadth is the maximum distance between the trochlear margins parallel to the coronal plane.

6) The posterior trochlear breadth is the minimum breadth of the trochlear margins taken parallel to the coronal talar plane.

7) The long dimension of the head is defined as the length of the long dimension of the talo-navicular articulation of the head and is measured obliquely along its long axis.

8) The short dimension of the head is defined as the length of the short dimension of the talo-navicular articulation of the head and is measured at right-angles to the long dimension. This dimension includes the facet for the spring ligament where identifiable.

9) The maximum functional length is the measured distance length from the groove for the tendon of the muscle flexor hallucis longus posteriorly to the intersection of the talar neck plane and the articular surface for the navicular.

10) The maximum breadth is measured from the tip of the lateral tubercle to the medial talar margin. The dimension is taken in the coronal talar plane.

11) The trochlear chord is the length of the chord connecting the intersections of the median trochlear arc and the anterior and posterior margins of the superior trochlear facet.

12) The medial facet length is the maximum distance between the anterior border and posterior tip of the medial facet.

13) The overall medial trochlear length is the maximum distance between the anterior tip of the medial facet and the posterior extreme of the medial trochlear surface.

14) The lateral facet length is defined as the maximum distance between the anterior

and posterior borders of the lateral facet at their intersection with the superior trochlear surface.
15) The talar neck length is defined as the maximum distance from the intersection of the median trochlear arc and the anterior border of the trochlear facet, to the intersection of the talar neck plane and the distal extremity of the navicular articulation.
16) The maximum neck diameter is the diameter of the talar neck measured obliquely, coinciding with the long axis of the head.
17) The minimum neck diameter is the diameter of the talar neck measured at right angles to above, coinciding with the short axis of the head.
18) The calcaneal facet dimension is defined as the maximum span of the calcaneal facet.
19) The talar neck-body angle is defined as the angle subtended by the intersection of the median sagittal talar plane and the median talar neck plane.
20) The talar head torsion angle is defined as the angle subtended by the long bisection of the talar head and the trochlear-head plane measured on a digital photographic image. In order to allow accurate measurement of the talar head torsion angle, the talus was carefully positioned with its neck in line with the camera. This ensures that the true torsion angle is obtained and that it is not distorted due to it's alignment with the camera.

The Calcaneus

The standard calcaneal basal plane may be defined as the position assumed by the calcaneus when it is resting upon the medial and (if present) lateral tubercles posteriorly and the plantar-most tip of the cuboid facet anteriorly.

The median sagittal calcaneal plane is the sagittal plane which passes along the long axis of the calcaneal tuber perpendicular to the standard calcaneal basal plane, effectively dividing it into two equal parts.

The coronal calcaneal plane is the coronal plane which passes from the most medial point of the sustentaculum tali laterally, perpendicularly to the other two planes

The median calcaneal tuberosity plane is the plane which lies in the midline of the long axis of the calcaneal tuberosity. In humans it closely approximates the median sagittal plane but is markedly oblique to this plane in hominoids due to torsion of the calcaneal tuber.

The talar facet plane is the plane defined by the most superior margins of the articular surface for the talus. This plane may be defined by the positioned assumed by the inverted calcaneus resting upon the talar articular surface.

1) The maximum length is the linear measurement from the most posterior point on the calcaneal tuber to the most anterior point on the superior edge of articular surface for the cuboid.
2) The sustentaculum breadth is the projected linear measurement taken from the most medial point on the sustentaculum tali to the most lateral point on the posterior talar articular facet.

3) The calcaneal body is the linear dimension between the most anterior part of the posterior talar facet to the most posterior point of the tuberosity.
4) The overall articular dimension is the projected distance between the most posterior part of the posterior talar facet to the anterior margin of the anterior facet.
5) The minimum tuber breadth is the minimum dimension from the most medial to the most lateral surfaces of the calcaneal tuber and is taken posteriorly to the talar articulations.
6) Tuberosity breadth is defined as the maximum distance between the medial and lateral margins of the tuberosity.
7) The posterior talar articular surface a: length is measured from the antero-lateral to postero-medial margins along the long axis of the facet
8) The posterior talar articular surface b: breadth is measured from the antero-medial to the postero-lateral margins perpendicular to (7) above.
9) The dorso/plantar cuboid facet dimension is the projected measurement from the most dorsal to the most plantar margins of the cuboid facet.
10) The medio/lateral cuboid facet dimension is taken at right angles to the dorso/plantar cuboid facet dimension (9), and is from the most medial to the most lateral margins of the facet.
11) The sustentaculum tali projection is the measurement of the distance the sustentaculum projects medially from the surface of the calcaneus.

Analytical Methods

Initially a univariate analysis was undertaken in which the spreads of the individual values for each dimension were compared in each species group. In addition, the standard univariate descriptors: mean, standard deviation, coefficients of variation and distribution shape, were scrutinised. This preliminary analysis had three key objectives. First, it is an essential step in interpretation of subsequent multivariate analyses. Second, it is a most useful way of identifying wrongly recorded data, for instance a misplaced decimal point. Third, it gives a broad comparison of size differences between the groups. Subsequently, Student's *t*-test was undertaken to investigate significance of differences of means between groups.

Plots of means against their standard deviations showed a strong positive regression for most dimensions. The data were subsequently transformed to their natural logarithms. A series of similar plots using the transformed data did not show a significant regression in the vast majority of variables. It was, therefore, considered wise to use log transformed data for the subsequent multivariate analyses.

The multivariate objective of the study was to establish the morphological affinities between the groups using canonical variates analysis (*43-45*).

Computations were undertaken using PC SAS 9.1 (SAS, 1988) and produced four standard outputs for subsequent scrutiny: mean values for each group on each canonical axis, eigenvalues of each canonical axis (indicating the proportion of total information contained within the axis), canonical coefficients, and Mahalanobis' D^2 distance matrix (SOM tables S3, S4, S6 and S7).

Indices were constructed from linear data (SOM tables S8 and S9). The primary reason for using indices, however, was not to remove the gross effects of size, but to emphasize biomechanically important aspects of the osseous morphology. The problems associated with the use of indices to deal with size are well recognized (*46, 47*). Where, however,

the intention is primarily to emphasize features thought to be mechanically important rather than as a deliberate attempt to remove the effect of ‘‘size’’, their use is essential. Plots of the mean scores of each group on the first canonical variate against the scores on second and third variates were constructed in order to gain a visual impression of the relationships between the groups. Two analyses were undertaken on the calcaneus to allow at least a rudimentary comparison with the previous OH 8 study (which has a highly fragmented calcaneus). First, an analysis utilising the three available indices was undertaken (the original OH 8 study used one further dimension, the cuboid facet angle; it was felt that the U.W. 88 calcaneus was not of sufficient preservation to capture this dimension) on both OH 8 and U.W. 88-99. Subsequently a new series of indices were defined (including those already used), and a second analysis was undertaken.

TABLES

Table S1: Structure matrix for canonical discriminant analysis of distal tibia. 88.1% of the individual distal tibiae were correctly identified using this discriminant function. The Malapa hominins were grouped with *Homo sapiens* among extant taxa and with fossil *Homo* among fossil taxa.

	Function 1	Function 2	Function 3
% of discrimination	68.8%	21.8%	8.3%
Variable			
Metaphyseal width (ML)	.092	.111	-.261
Metaphyseal width (AP)	-.507	.182	-.037
Medial malleolus width (ML)	.593	.057	.114
Medial malleolus height (SI)	.112	.506	.742
Medial malleolus length (AP)	-.063	.360	-.476
Anterior articular surface (ML)	.410	.003	-.280
Midpoint articular surface (ML)	.036	-.520	-.189
Posterior articular surface (ML)	-.227	-.687	.111
Medial articular surface (AP)	-.005	-.400	-.100
Midpoint articular surface (AP)	-.026	.219	-.256
Lateral articular surface (AP)	-.350	-.237	.029

Table S2. Mean talar neck and head torsion angles and standard deviations (in parentheses) of humans and extant apes used in this study and comparative fossil specimens including the *Au. sediba* talus *U.W. 88-98*.

	Neck angle	Head torsion angle
Homo female (n=20)	18.9 (2.6)	42.2 (5.4)
Homo male (n=20)	18.6 (2.5)	44.2 (4.8)
Pan female (n=20)	32.4 (4.4)	24.5 (6.2)
Pan male (n=20)	29.8 (4.4)	26.1 (4.8)
Gorilla female (n=20)	32.4 (4.2)	19.7 (5.9)
Gorilla male (n=20)	31.5 (5)	21.5 (3.3)
Pongo female (n=17)	33.9 (6)	7.5 (6.4)
Pongo male (n=10)	27.6 (4.6)	8.6 (4.7)
U.W. 88-98	28	15
StW 573	31.3	26.1
StW 88	32	22
SKX 42695*	35	30
OH 8	33.5	28.5
A.L. 288-1	33.4	28.6
KNM-ER 1464	19.8	24.2

*Estimate based on reconstruction of the talar head.

Table S3. Indices of talar dimensions (SOM textS3). Adapted from Kidd *et al. (40)*.

Index	Anatomical description	Suggested mechanical Implication
1: Medial talar height/lateral talar height	Trochlear surface morphology	Set of tibia on foot Possible Indicator of the degree of foot pronation
2: Median talar height/medial talar height		
3: Median talar height/transverse trochlear breadth	Relative breadth	Possible indicators of body mass
9: Minimum neck dimension/ maximum neck dimension	Overall neck thickness	
4: Anterior trochlear breadth/ posterior trochlear breadth	Trochlear wedging	Possible indicators of direction and degree of ankle movement and loading environment.
8: Medial facet length/lateral facet length	Trochlear morphology	
5: Short head dimension/long	Head articular morphology	Possible indicator of degree and direction of talonavicular movement
6: Maximum talar breadth/ maximum talar length	Overall bone morphology	Possible indicator of overall foot length
10: Talar neck angle	Degree of ray divergence	Possible indicator of presence or absence of divergent first ray (indicator of degree of arboreality)
7: Trochlear cord/maximum	Relative neck length	
11: Talar head torsion angle	Orientation of talo-navicular axis	Possible indicator of effectiveness of midtarsal restraining mechanism

Table S4: The eigenvalues, pooled within-class standardized canonical coefficients and percentages of discrimination for the canonical variates analysis of hominoid tali including *U.W. 88-98*. Three indices in particular contribute to the discrimination along the second variates, 2, 4 and 6. Index 4 describes the degree of trochlear wedging while index 6 is a measure of relative bone length and breadth.

		Can 1	**Can 2**	**Can 3**
Eigenvalue		7.48	5.19	0.96
% of discrimination		53.23	36.94	6.85
Coefficients	Index 1	0.858	0.348	-0.442
	Index 2	0.486	0.476	-0.567
	Index 3	-0.112	0.329	0.759
	Index 4	-0.076	-0.480	0.252
	Index 5.	-0.076	-0.015	0.373
	Index 6	-0.017	0.545	-0.253
	Index 7	0.391	0.094	0.222
	Index 8	-0.091	0.138	-0.006
	Index 9	0.183	0.209	0.402
	Index 10	-0.648	0.373	0.229
	Index 11	0.429	0.212	0.039

Table S5. Talar and calcaneal group means along canonical variates one, two, three.

		Talus (U.W. 88-98)			Calcaneus (U.W. 88-99)		
Group	Sex	Can 1	Can 2	Can 3	Can 1	Can 2	Can 3
% of total Discrimination		53.23	36.94	6.85	51.65	35.65	9.41
Fossil		1.618	-0.669	5.175	1.102	0.527	0.746
Homo	F	3.568	-1.826	-0.374	2.109	-1.821	-0.020
Homo	M	3.615	-1.607	-0.404	2.282	-1.656	-0.111
Pan	F	-0.370	1.185	1.234	-0.881	-0.051	0.918
Pan	M	0.245	1.293	1.289	-1.220	0.414	1.398
Gorilla	F	-1.378	2.373	-0.684	0.437	2.487	-0.176
Gorilla	M	-0.419	2.847	-1.142	1.327	2.215	-0.759
Pongo	F	-5.022	-3.223	-0.293	-2.826	-0.976	-1.149
Pongo	M	-2.147	-2.986	0.146	-3.328	-1.073	-0.654

Table S6. Mahalonobis D^2 distances from the fossil to group centroids of the tali and calcaneii.

	Sex	U.W. 88-98 Talus	U.W. 88-99 Calcaneus
Fossil		0	0
Homo	F	45.75	14.21
Homo	M	42.78	11.96
Pan	F	32.96	11.39
Pan	M	28.54	11.27
Gorilla	F	62.65	11.04
Gorilla	M	61.66	11.70
Pongo	F	88.69	26.19
Pongo	M	52.00	31.72

Table S7. Measurements of the calcanei of extant and extinct hominids including *U.W. 88-98* of *Au. sediba*. Data from Latimer and Lovejoy (*20*) with updated body masses from Smith and Jungers (*48*). *Au. afarensis* body mass estimates were based on the masses predicted for the largest weight-bearing joints from the Hadar 333 site in McHenry (*49*), making this the most conservative estimate (smaller body mass estimate would make the tuber volume/body mass ratio *higher* and thus more human-like). Body mass estimates of *U.W. 88-98* were based on the very same regression equations found in McHenry (*49*) on the articular surface of the associated talus, tibia, and femoral head of MH 2. Note that although the calcaneal tuber is relatively larger in *Au. sediba* than in African apes, it is smaller than both modern humans and *Au. afarensis*. Though we hypothesize that this is a real difference between the two fossil hominins, how much variation exists in the calcaneal body and the range of overlap in this measure will have to await discovery of additional calcanei from *Australopithecus*.

	Posterior talar facet subtended angle (° ± SD)	**Minimal cross-sectional area (cm^2 ± SD)**	**Length of tuber (cm ± SD)**	**Minimal tuber volume (cm^3 ± SD)**	**Body mass (kg)**	**Tuber volume/body mass (cm^3/kg)**
Pan Male	110.0 ± 9.3	3.0 ± 0.4	3.7 ± 2.6	10.8 ± 0.9	49.6	0.22
Pan Female		3.0 ± 0.4	3.4 ± 2.5	10.1 ± 1.6	40.4	0.25
Gorilla Male	100.0 ± 8.2	5.8 ± 0.6	6.1 ± 2.5	35.2 ± 3.7	172.8	0.20
Gorilla Female		3.1 ± 0.5	5.1 ± 2.5	16.0 ± 3.0	71.3	0.23
Homo sapiens Male	78.5 ± 10.0	10.0 ± 1.8	5.4 ± 3.2	53.1 ± 10.9	68.2	0.78
Homo sapiens Female		7.9 ± 1.0	4.9 ± 3.0	38.7 ± 5.5	55.0	0.70
Australopithecus afarensis(A.L. 333-8)	82.0	7.0	4.0	28.1	42.7-50.1	0.56-0.66
Australopithecus sediba(UW 88-98)	118.3	3.5	3.8	13.4	25.8-34.9	0.38-0.52

Table S8. Indices of calcaneal dimensions.

Index	Anatomical description	Suggested mechanical Implication
1: Sustentaculum breadth/ Maximum length	Relative facet breadth and morphology	Amount of magnitude of talar facets compared to calcaneal size
2: Sustentaculum breadth/ overall articular dimension		Possible indicator of body mass
3: Calcaneal body/ Maximum length	Reletive magnitude of body as a proportion to total length	Lever arm implying degree of bipedality
4: Overall articular dimension/ maximum length.		
5: Minimum tuberosity breadth/ maximum tuberosity breadth.	Tuberosity morphology	Calcaneal body robusticity
6: Tuberosity breadth/ maximum calcaneal length.		
7: Posterior talar facet: breadth/length	Facet morphology	Possible indicator of direction of movement at subtalar joint
8: Cuboid facet: mediolateral/ dorsoplantar	Facet morphology	Relative robusticity and possible indicator of stability at the calcaneocuboid joint

Table S9: The eigenvalues, pooled within-class standardized canonical coefficients and percentages of discrimination for the canonical variates analysis of hominoid calcanei including *U.W. 88-99*. Indices 1 and 6, and to a lesser extent 4 are predominant in the discrimination along variate 1. These describe the relative length and breadth of the bone, the relative tuberosity morphology, and the relative bone length. Along variate 2, indices 1, 7 and to a lesser extent 5 are the most prominent. Index 7 describes the posterior talar facet morphology and 5, the relative tuber breadth.

		Can 1	**Can 2**	**Can 3**
Eigenvalue		3.83	2.64	0.70
% of discrimination		51,65	35,63	9,41
Coeffiients	Index 1	-0.704	0.531	0.615
	Index 2	0.407	0.042	0.111
	Index 3	0.100	0.356	-0.146
	Index 4	0.000	0.000	0.000
	Index 5.	0.327	-0.452	0.619
	Index 6	0.889	0.199	0.157
	Index 7	-0.326	0.704	-0.107
	Index 8	0.021	0.269	-0.025

FIGURES

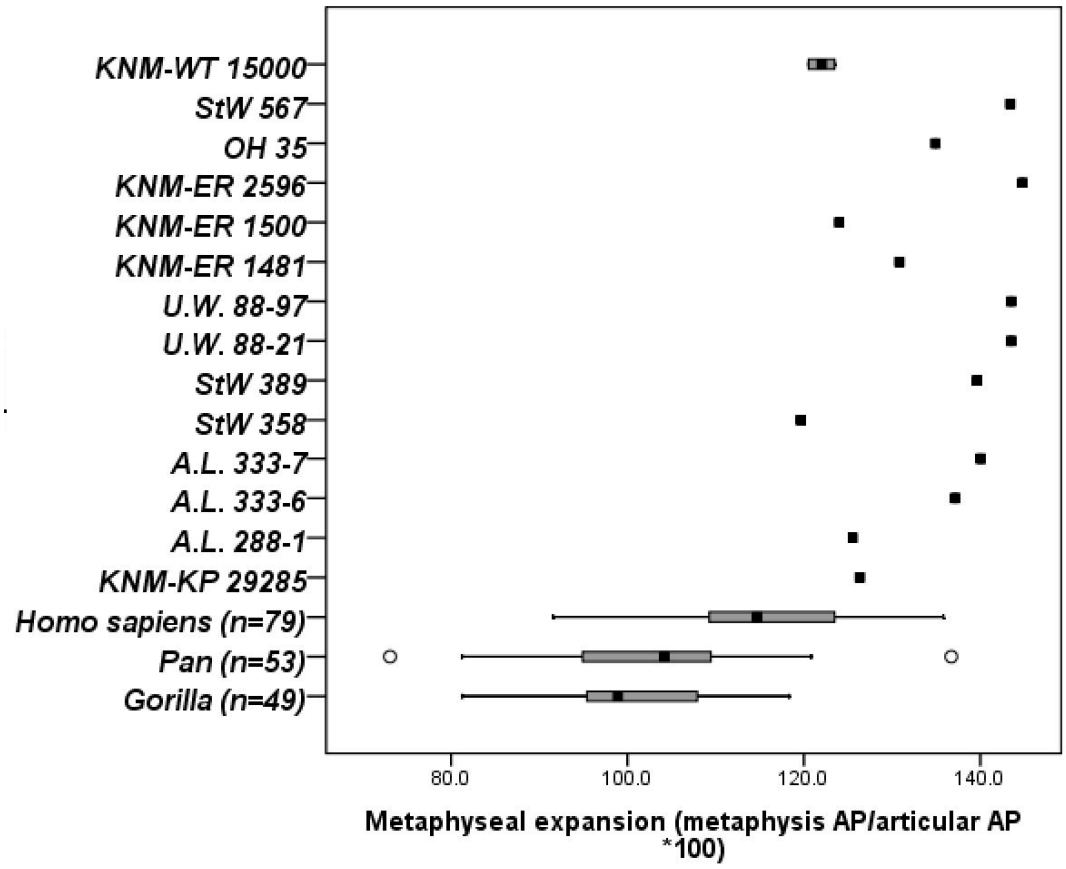

Fig. S1. Metaphyseal expansion**.** Relative to the articular surface, humans and especially fossil hominins have an anteroposteriorly expanded metaphysis, thought to be important for strain dissipation during bipedality. *Au. sediba* is like other hominins for this parameter. This ratio was taken as the maximum anteroposterior dimension of the distal tibial metaphysis divided by the anteroposterior length of the distal tibial articular surface at the midpoint of the joint. In this, and in all future graphs, the mean is indicated by the dark line, the interquartile range by the boxes, the full range of data by the whiskers, and outliers are circles.

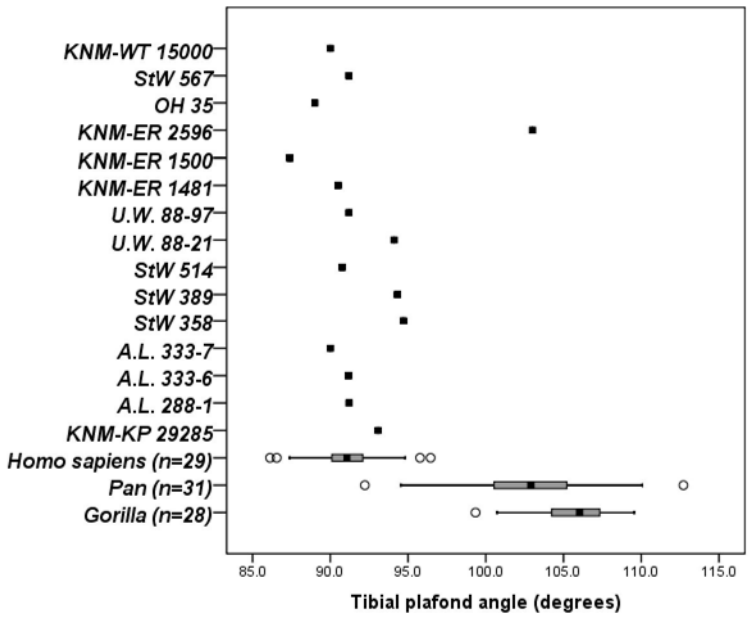

Fig. S2. Humans have perpendicularly oriented ankle joint (in the coronal plane) relative to the tibial shaft. This positions the knee over the ankle and is indirectly correlated with a valgus knee. All hominins (including *Au. sediba*) are human-like, except pathological ones (KNM-ER 2596). See Latimer et al. (*51*), DeSilva (*12*) for methods detailing the tibial plafond angle measurement. See DeSilva and Papakyrikos (*51*) for description of the KNM-ER 2596 fossil.

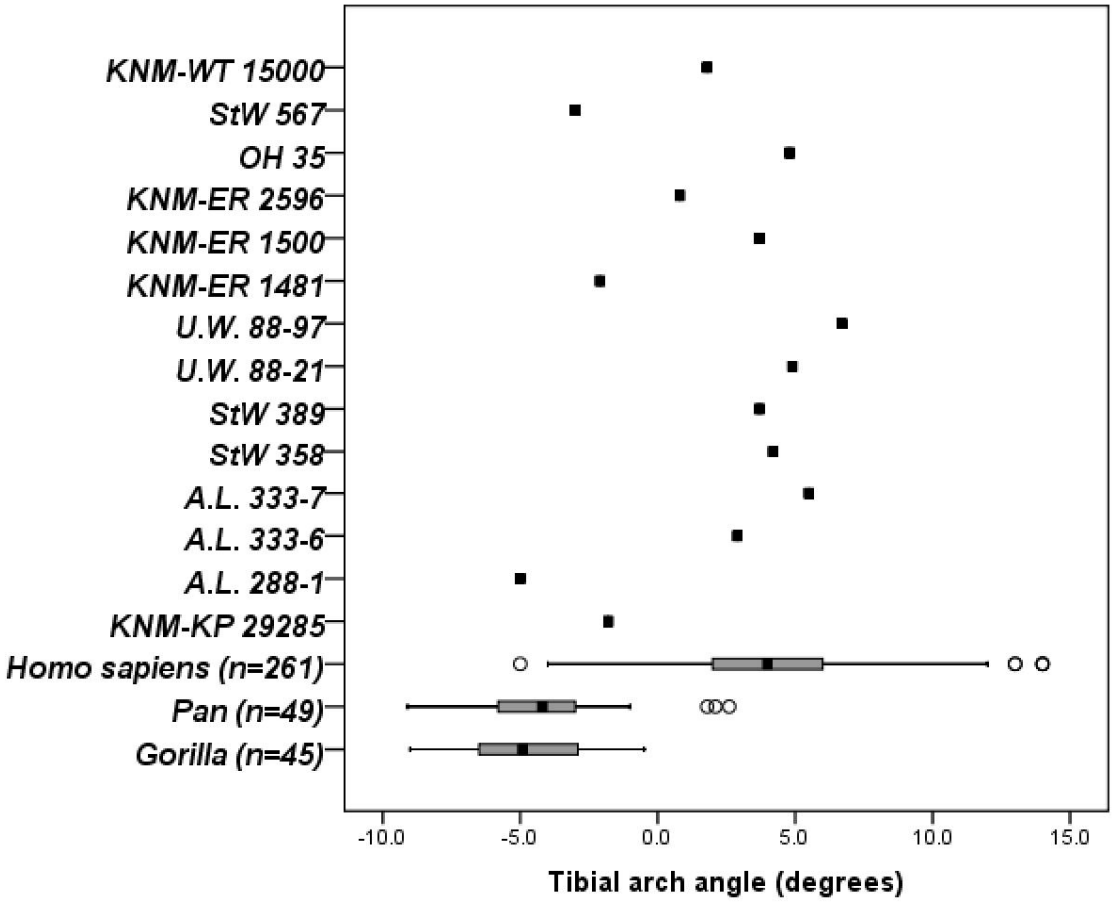

Fig. S3. The angle the tibial plafond forms with the tibial shaft in the sagittal plane. This may be related to rearfoot arching (*13*). The humans and fossil hominins that have a more negative set may have had non-pathological flatfeet. The Malapa hominins have an angle suggestive of rearfoot arching (consistent with talar neck inclination, and calcaneocuboid joint facet angle).

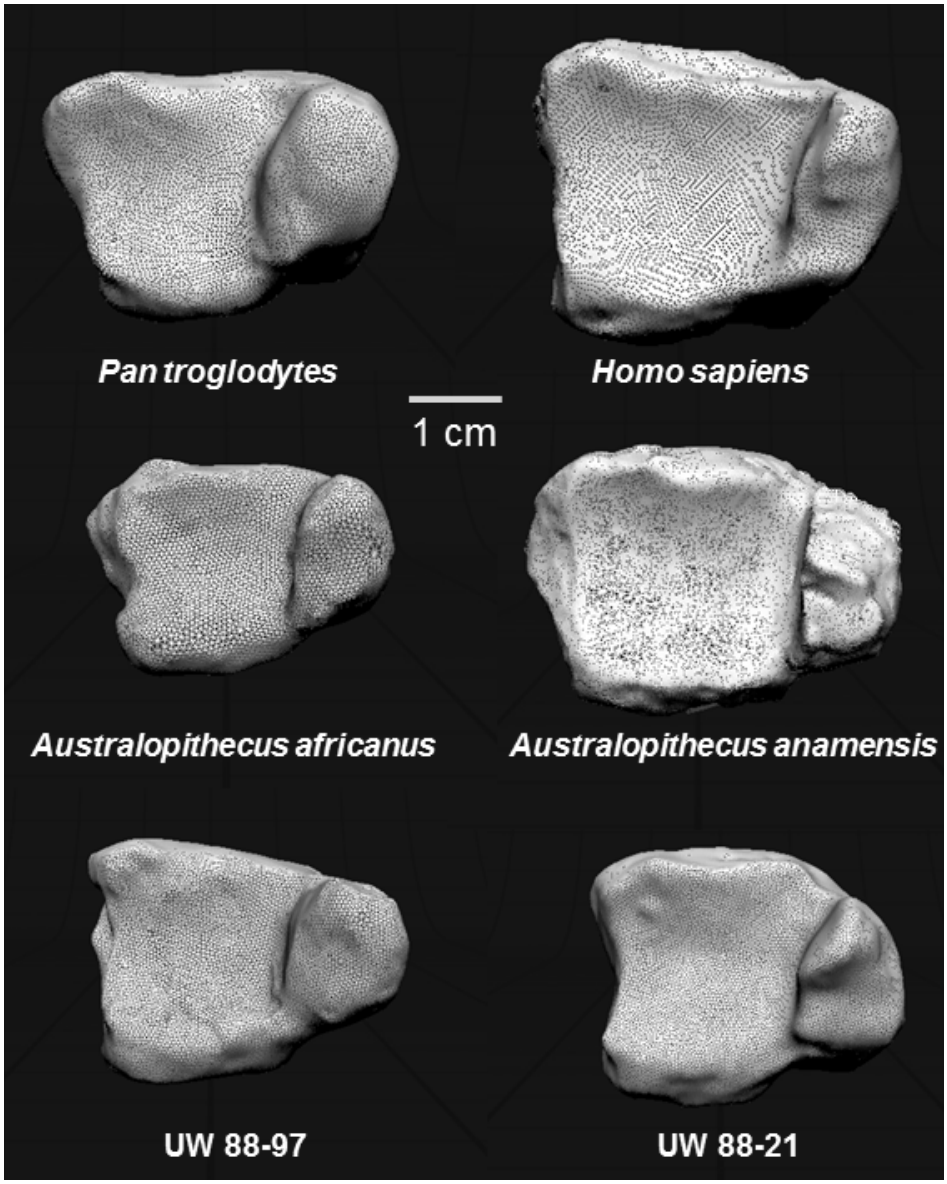

Fig. S4. Distal tibia in inferior view. In this image, StW 358 represents *Au. africanus* and KNM-KP 29285 is the *Au. anamensis* tibia. StW 358 has been reversed so that all appear from the right side. Notice the trapezoid shaped plafond in the chimpanzee and the more rectangular/square shape in humans and fossil hominins. The medial malleolus is extremely thick in chimpanzees and in the Malapa hominins, and moderately thick in *Au. africanus*. It is thin in humans and in most *Australopithecus*. Scale bar = 1cm.

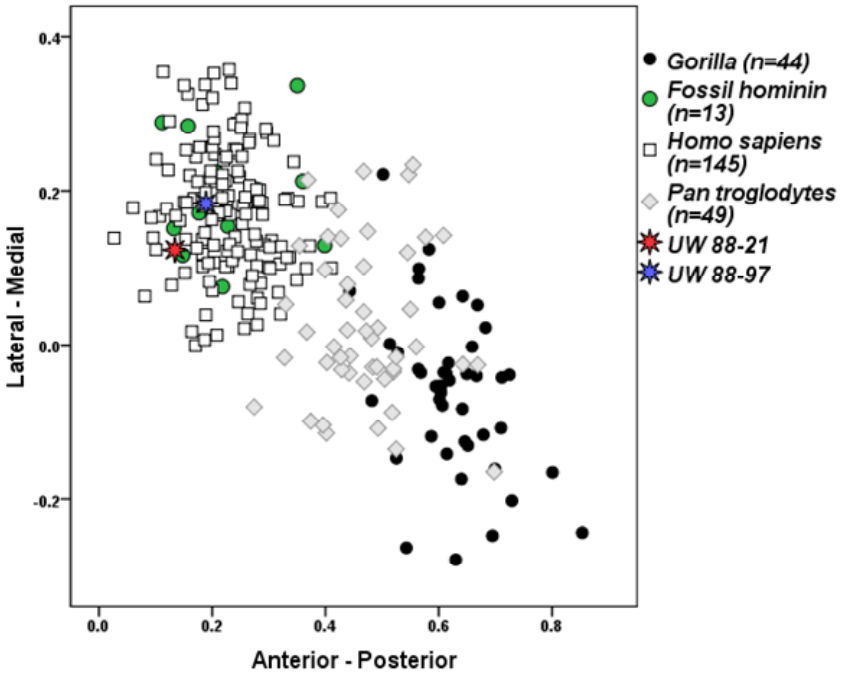

Fig. S5. The dimensions of the tibial plafond were size standardized (see DeSilva (*12*) for details of methods). Subtracting the posterior from the anterior dimension, and the medial from the lateral, separates the African apes from modern humans. Fossil hominins, including the Malapa individuals are quite human-like for the geometry of the tibiotalar joint, indicating that only the thickened medial malleolus distinguishes *Au. sediba* tibiae from human and hominin tibiae.

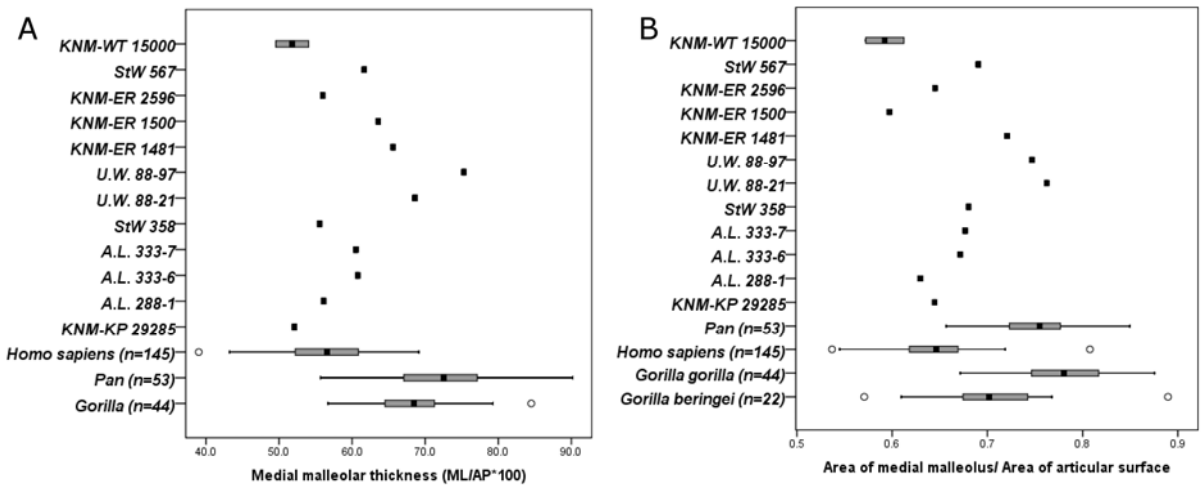

Fig. S6. Two different measures of the relative size of the medial malleolus demonstrate that climbing apes have a thicker malleolus than bipedal humans. A: The maximum mediolateral thickness of the medial malleolus is divided by the maximum anteroposterior length of the malleolus in humans, apes, and fossil hominins. The medial malleoli of the Malapa hominins are remarkably thick, beyond the range of modern humans or fossil hominins and instead are quite like the thick malleolus in apes. B: The cross sectional area of the medial malleolus (mediolateral width * anteroposterior length) was divided by the area of the talar articular surface of the distal tibia (anteroposterior width taken at midpoint * mediolateral width taken at midpoint of joint). Again, the two *Au. sediba* tibiae have the largest medial malleolus of the entire hominin fossil sample and are the only hominins entirely outside the human range (though KNM-ER 1481 is close). Importantly, the almost exclusively terrestrial mountain gorilla has a relatively *thinner* medial malleolus, statistically smaller ($t=5.26$, $p<0.001$) than the medial malleolus in the more arboreal lowland gorilla. A thick medial malleolus may suggest an ankle loaded in inversion, and some climbing in *Au. sediba*.

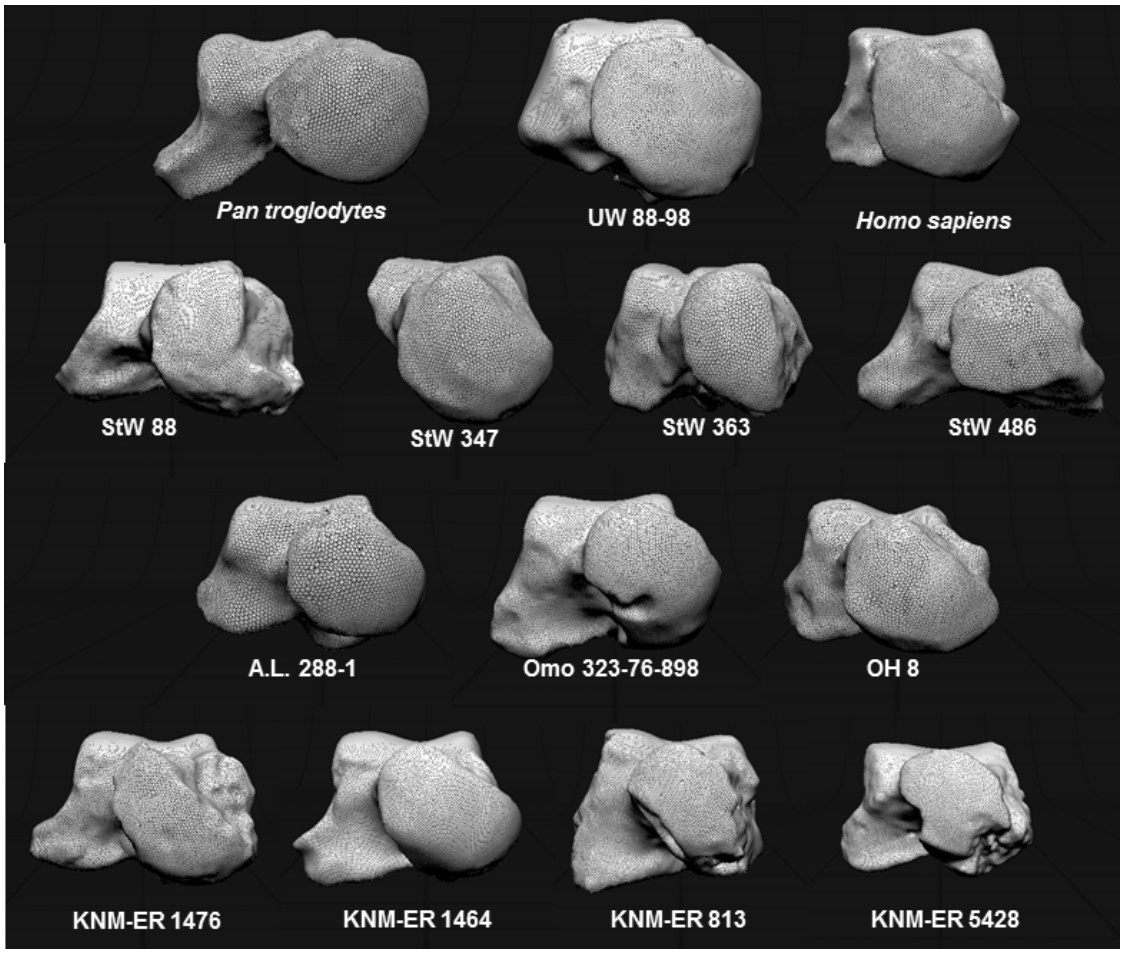

Fig. S7. Fossil hominin tali in distal view. Left tali have been reversed so that they all appear from the right side. All tali have been scaled so that the trochlear body is the same mediolateral width. There is tremendous variation in the torsion angle of the head, and in the grooving of the trochlea in fossil hominins. Notable in this orientation is the remarkably large talar head of *U.W. 88-98*.

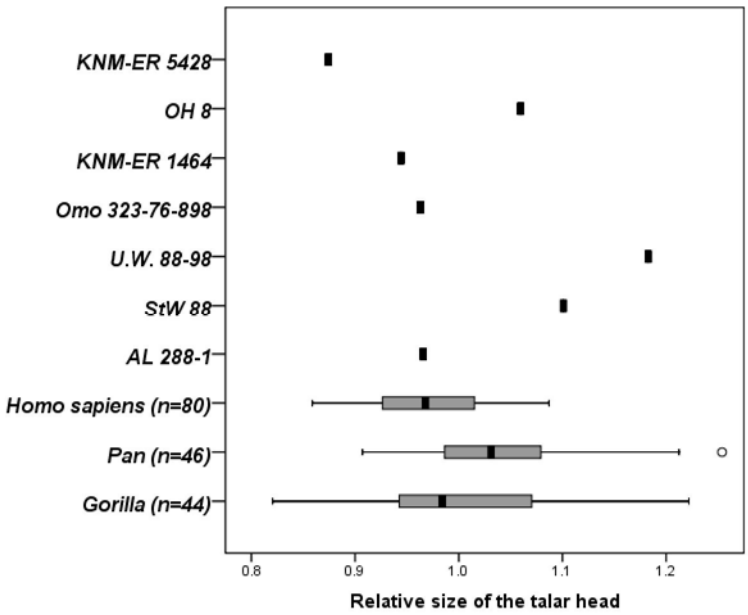

Fig. S8. The *Australopithecus sediba* talus possesses a disproportionately large talar head relative to the dimensions of the talar body. The squareroot of the product of the maximum mediolateral width (along the torsional axis) and dorsoplantar height (perpendicular to the width) of the talar head was divided by the mediolateral width at the anterioposterior midpoint of the talar body. The fossil hominins preserved well enough for this measure (A.L. 288-1, StW 88, Omo 323-76-898, OH 8, KNM-ER 1464, and KNM-ER 5428) fall within or near (e.g. StW 88) the modern human range for these proportions. *U.W. 88-98* is unique in having a relatively large talar head, barely within the range of the African apes. A t-test showed no significant difference between male and female gorillas ($p=0.33$) or chimpanzees ($p=0.85$), suggesting that this is not a size related feature and instead may indicate mobility at the talonavicular joint.

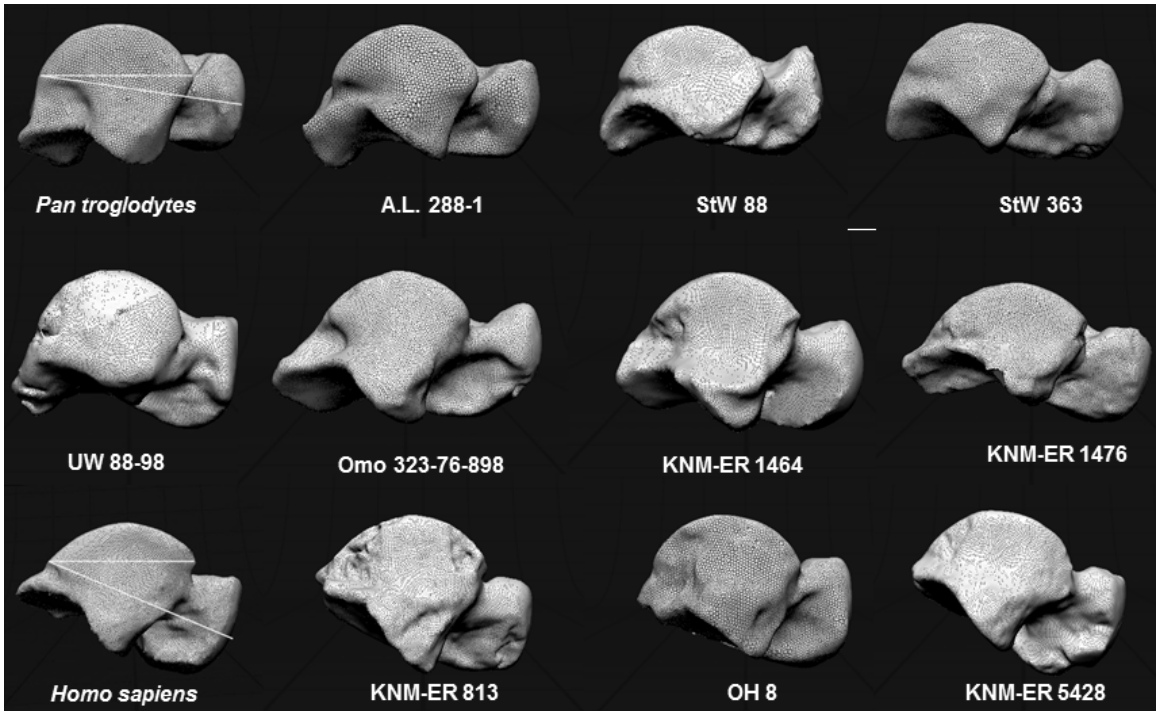

Fig. S9. Fossil hominin tali in lateral view. Left tali have been reversed so that they all appear from the right side. Each talus has been oriented so that a straight line can be drawn through the most proximal and the most distal extent of the trochlear surface (as shown by the white line in the chimpanzee and human tali, and all tali have been scaled so that this line is the same length throughout). Relative to this line, the talar head and neck are inclined plantarly in most humans, fossil *Homo* (OH 8, KNM-ER 813, KNM-ER 5428) and in *U.W. 88-98*, as indicated by the line bisecting the talar head and neck. This plantar inclination is suggestive of rearfoot arching.

A

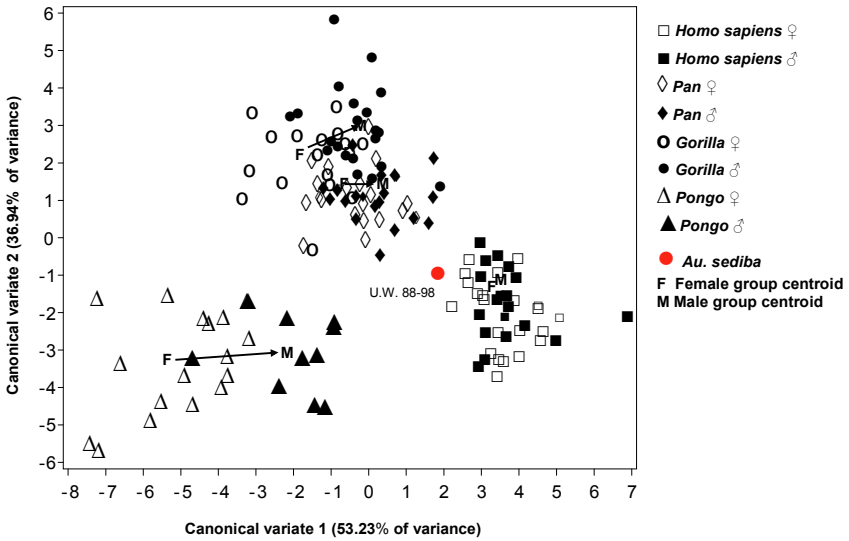

B

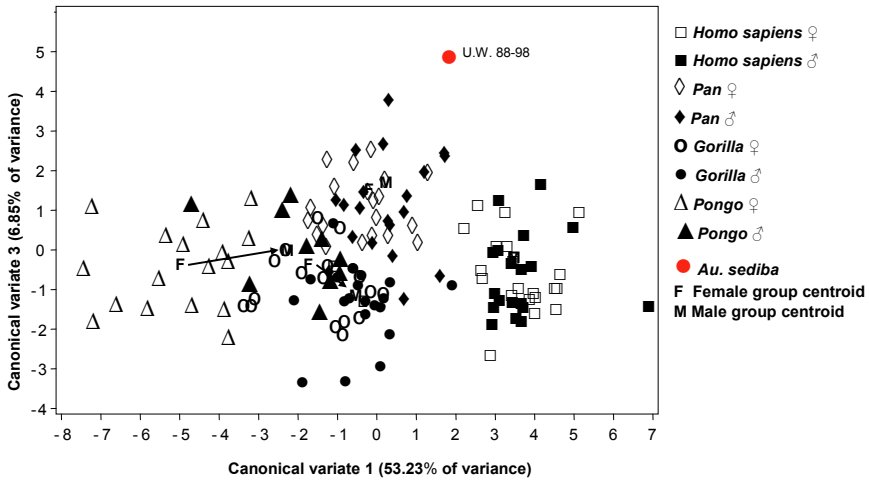

Fig. S10. Canonical variates analysis of the talus using 11 variables. **(A)** Plot of canonical means along canonical variates one and two (apes, humans and fossil) shows a discrimination of *U.W. 88-98* between the African apes and humans. **(B)** Plot of canonical means along canonical variates one and three (apes, humans and fossil) places *U.W. 88-98* in a unique position unlike the apes and humans. *Homo, Pan and Gorilla* (n = 20 males; 20 females) and *Pongo* (n = 10 males; 17 females).

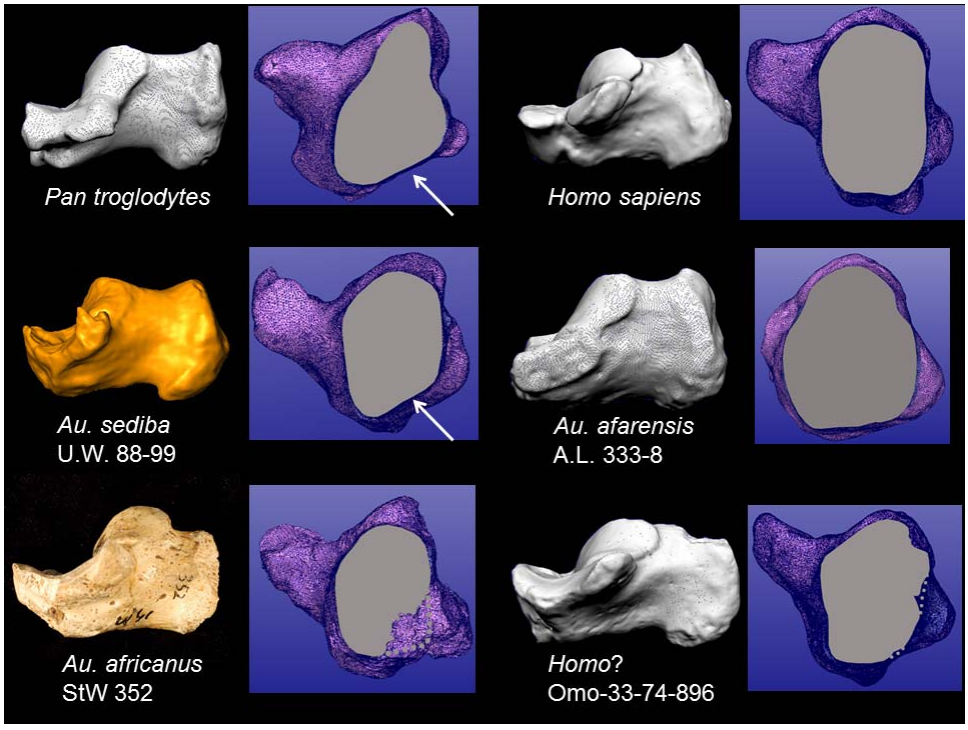

Fig. S11. The calcaneus of a chimpanzee, human, and four fossil hominins are shown in medial view. 3-D scans of the calcanei were acquired using a NextEngine desktop scanner and the tuber was digitally cross-sectioned at the point of the minimum circumference following Latimer and Lovejoy (*20*) using DeskArtes Dimensions Expert. Humans, and all fossil hominins (including *Au. sediba*) have a mediolaterally broad tuber in cross-section, thought to be an adaptation for bipedal locomotion. However, unlike modern humans, *Au. afarensis* and the calcaneus from Omo, the lateral plantar region is angled (indicated with an arrow) and not robust in *Au. sediba*. In this respect, the fossil is ape-like. Unfortunately, there is no *Au. africanus* calcaneus with a complete tuber. However, StW 352 (from Member 4 and therefore most likely *Au. africanus*) has enough of a tuber preserved to acquire the medial aspect of this cross-section and to estimate the lateral side. Note that what is present is broader than the *Au. sediba* plantar region and that bone located distally to the tuber (outline in gray dots; colored purple) strongly suggests that the tuber was expanded plantarly as is the case in the calcanei from Hadar and from Omo.

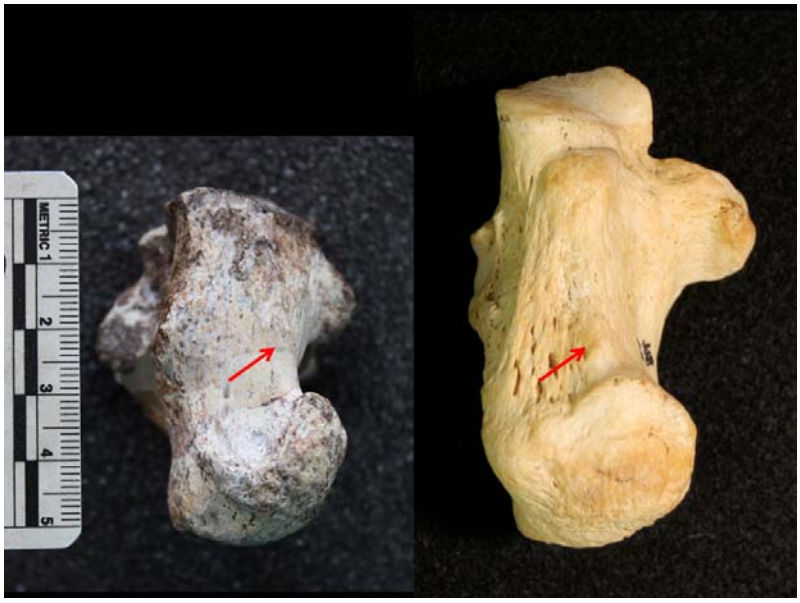

Fig. S12. On the left is a plantar view of the *U.W. 88-99* calcaneus compared to a modern human (right). Though both in plantar view, they are not oriented the exact same way and thus one should not infer morphology beyond what is intended with this image. The red arrows reference a small tubercle positioned just anterior to the medial plantar tubercle in both humans and in *Au. sediba* and is suggested here to reflect an attachment for the long plantar ligament. This tubercle was not detected on any African ape calcanei studied (n=15). Closer to the calcaneocuboid joint is a large rugosity (anterior tubercle) for the short plantar ligament, present in apes, humans, and *Au. sediba*.

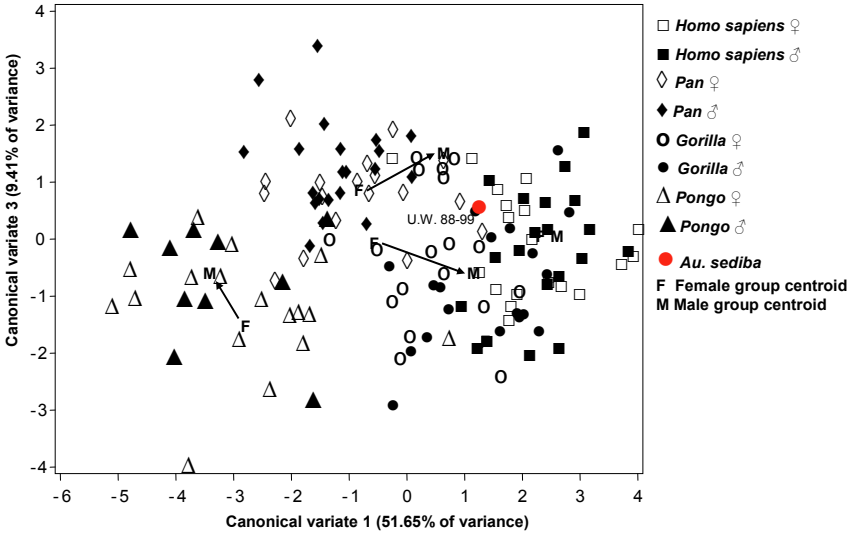

Fig. S13. Canonical variates analysis of the calcaneus using 8 indices (SOM text S3, Table S). Plot of canonical means along canonical variates one and three (apes, humans and fossil) shows a discrimination of *U.W. 88-99*, humans and the African apes from orang-utans. *Homo, Pan and Gorilla* (n = 20 males; 20 females) and *Pongo* (n = 10 males; 17 females).

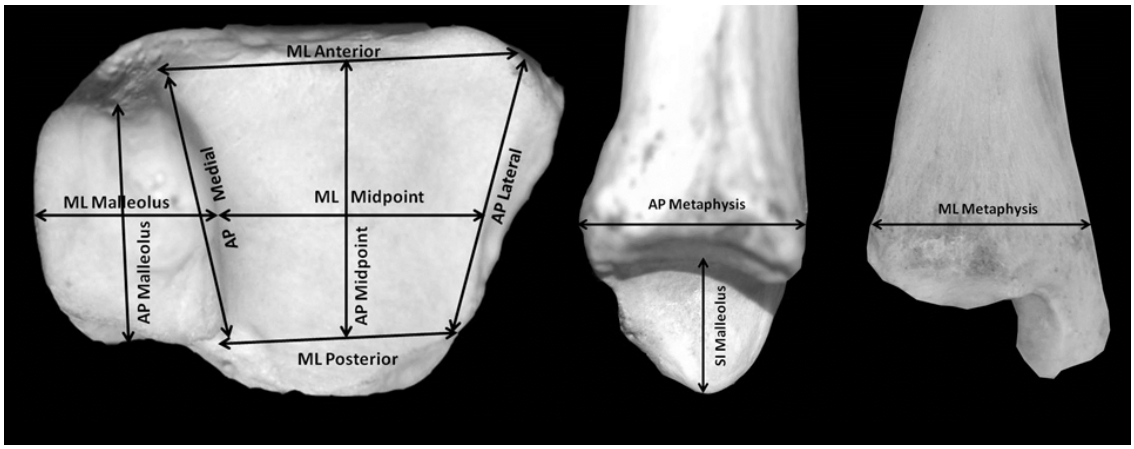

Fig. S14. Measurements taken on the distal tibia for univariate and discriminant functions analyses.

References and Notes

1. O. J. Lewis, The joints of the evolving foot. Part III. The fossil evidence. *J. Anat.* **131**, 275 (1980). Medline

2. D. J. Morton, *The Human Foot: It's Evolution, Physiology, and Functional Disorders* (Columbia Univ. Press, New York, 1935).

3. F. W. Wood Jones, *Structure and Function as Seen in the Foot* (Bailliere, Tindall and Cox, London, 1944).

4. M. H. Day, J. R. Napier, Fossil foot bones. *Nature* **201**, 969 (1964). doi:10.1038/201969a0 Medline

5. R. L. Susman, Evolution of the human foot: Evidence from Plio-Pleistocene hominids. *Foot Ankle* **3**, 365 (1983). Medline

6. W. E. Harcourt-Smith, L. C. Aiello, Fossils, feet and the evolution of human bipedal locomotion. *J. Anat.* **204**, 403 (2004). doi:10.1111/j.0021-8782.2004.00296.x Medline

7. L. R. Berger *et al*., *Australopithecus sediba*: A new species of *Homo*-like australopith from South Africa. *Science* **328**, 195 (2010). doi:10.1126/science.1184944 Medline

8. P. H. G. M. Dirks *et al*., Geological setting and age of *Australopithecus sediba* from southern Africa. *Science* **328**, 205 (2010). doi:10.1126/science.1184950 Medline

9. The absence of an epiphyseal line in the U.W. 88-21 right distal tibia suggests that it is not from a juvenile and therefore is unlikely to be from MH1. The remainder of the MH1 skeleton's dental and epiphyseal development is consistent with the age originally described (*7*). This tibia also does not belong to MH2, as the right tibia U.W. 88-97 (bound by matrix to the talus and calcaneus) is clearly directly associated with this individual.

10. Most of the comparative linear dimensions used in this study were collected on the original fossils using digital sliding calipers. To maximize measurement comparability and justify performing statistical analyses when pooling these data and data from the Malapa fossils, a high-resolution 3D printer was employed to produce 1:1 powder-based printouts from the renderings. The printouts were subsequently cast for distribution. Casts were validated by comparing measurements taken from exposed features of the original fossils with measurements taken from homologous features on the casts; differences were <0.5 mm. Measurements were taken on the casts following the same protocol as was applied when collecting the comparative data.

11. B. Latimer, J. C. Ohman, C. O. Lovejoy, Talocrural joint in African hominoids: Implications for *Australopithecus afarensis*. *Am. J. Phys. Anthropol.* **74**, 155 (1987). doi:10.1002/ajpa.1330740204 Medline

12. J. M. DeSilva, Functional morphology of the ankle and the likelihood of climbing in early hominins. *Proc. Natl. Acad. Sci. U.S.A.* **106**, 6567 (2009). doi:10.1073/pnas.0900270106 Medline

13. J. M. DeSilva, Z. J. Throckmorton, Lucy's flat feet: The relationship between the ankle and rearfoot arching in early hominins. *PLoS ONE* **5**, e14432 (2010). doi:10.1371/journal.pone.0014432 Medline

14. M. H. Day, B. A. Wood, Functional affinities of the Olduvai Hominid 8 talus. *Man (London)* **3**, 440 (1968). doi:10.2307/2798879

15. C. O. Lovejoy, in *Early Hominids of Africa*, C. E. Jolly, Ed. (Duckworth, London, 1978), pp. 403–429.

16. D. Kachlik *et al*., Clinical anatomy of the retrocalcaneal bursa. *Surg. Radiol. Anat.* **30**, 347 (2008). doi:10.1007/s00276-008-0335-4 Medline

17. G. Berillon, Assessing the longitudinal structure of the early hominin foot: A two-dimensional architecture analysis. *Hum. Evol.* **18**, 113 (2003). doi:10.1007/BF02436280

18. J. T. Stern Jr., R. L. Susman, The locomotor anatomy of *Australopithecus afarensis*. *Am. J. Phys. Anthropol.* **60**, 279 (1983). doi:10.1002/ajpa.1330600302 Medline

19. E. E. Sarmiento, Significance of the heel process in anthropoids. *Int. J. Primatol.* **4**, 127 (1983). doi:10.1007/BF02743754

20. B. Latimer, C. O. Lovejoy, The calcaneus of *Australopithecus afarensis* and its implications for the evolution of bipedality. *Am. J. Phys. Anthropol.* **78**, 369 (1989). doi:10.1002/ajpa.1330780306 Medline

21. B. Zipfel, J. M. DeSilva, R. S. Kidd, Earliest complete hominin fifth metatarsal—implications for the evolution of the lateral column of the foot. *Am. J. Phys. Anthropol.* **140**, 532 (2009). doi:10.1002/ajpa.21103 Medline

22. W. I. Sellers, T. C. Pataky, P. C. Caravaggi, R. H. Crompton, Evolutionary robotic approaches in primate gait analysis. *Int. J. Primatol.* **31**, 321 (2010). doi:10.1007/s10764-010-9396-4

23. All of the human calcanei that we studied possess this combination of an angled calcaneal tuber, Sharpey's fibers, and a flat surface for a bursa. No chimpanzees (n = 24) possessed these features together. However, these three features were found in a small number of gorilla calcanei (n = 5out of 25).

24. J. M. Kibii *et al*., A partial pelvis of *Australopithecus sediba*. *Science* **333**, 1407 (2011).

25. T. Kivell, J. M. Kibii, S. E. Churchill, P. Schmid, L. R. Berger, *Australopithecus sediba* hand demonstrates mosaic evolution of locomotor and manipulative abilities. *Science* **333**, 1411 (2011).

26. D. L. Gebo, Plantigrady and foot adaptation in African apes: Implications for hominid origins. *Am. J. Phys. Anthropol.* **89**, 29 (1992). doi:10.1002/ajpa.1330890105 Medline

27. R. E. Wunderlich, thesis, State University of New York, Stony Brook (1999).

28. J. M. DeSilva, thesis, University of Michigan (2008).

29. R. Pickering *et al*., *Australopithecus sediba* at 1.977 Ma and implications for the origins of the genus *Homo*. *Science* **333**, 1421 (2011).

30. M. G. Leakey, C. S. Feibel, I. McDougall, C. Ward, A. Walker, New specimens and confirmation of an early age for *Australopithecus anamensis*. *Nature* **393**, 62 (1998). doi:10.1038/29972 Medline

31. R. C. Walter, Age of Lucy and the first family: Single-crystal $^{40}Ar/^{39}Ar$ dating of the Denen Dora member of the Hadar Formation, Ethiopia. *Geology* **22**, 6 (1994). doi:10.1130/0091-7613(1994)022<0006:AOLATF>2.3.CO;2

32. R. Pickering, J. D. Kramers, Re-appraisal of the stratigraphy and determination of new U-Pb dates for the Sterkfontein hominin site, South Africa. *J. Hum. Evol.* **59**, 70 (2010). doi:10.1016/j.jhevol.2010.03.014 Medline

33. C. S. Feibel, F. H. Brown, I. McDougall, Stratigraphic context of fossil hominids from the Omo group deposits: Northern Turkana Basin, Kenya and Ethiopia. *Am. J. Phys. Anthropol.* **78**, 595 (1989). doi:10.1002/ajpa.1330780412 Medline

34. V. Balter *et al*., U-Pb dating of fossil enamel from the Swartkrans Pleistocene hominid site, South Africa. *Earth Planet. Sci. Lett.* **267**, 236 (2008). doi:10.1016/j.epsl.2007.11.039

35. R. J. Blumenschine *et al*., Late Pliocene *Homo* and hominid land use from Western Olduvai Gorge, Tanzania. *Science* **299**, 1217 (2003). doi:10.1126/science.1075374 Medline

36. A. C. Walker, R. E. F. Leakey, *The Nariokotome* Homo erectus S*keleton* (Harvard Univ. Press, Cambridge, MA, 1993).

37. R. Kidd, thesis, University of Western Australia (1995).

38. R. Kidd, The past is key to the present: thoughts on the origins of human foot structure, function and dysfunction as seen from the fossil record. *Foot* **8**, 75 (1998). doi:10.1016/S0958-2592(98)90002-5

39. R. Kidd, Evolution of the rearfoot. A model of adaptation with evidence from the fossil record. *J. Am. Podiatr. Med. Assoc.* **89**, 2 (1999). Medline

40. R. Kidd, P. O'Higgins, C. E. Oxnard, The OH8 foot: A reappraisal of the functional morphology of the hindfoot utilizing a multivariate analysis. *J. Hum. Evol.* **31**, 269 (1996). doi:10.1006/jhev.1996.0061

41. R. S. Kidd, C. E. Oxnard, Patterns of morphological discrimination in selected human tarsal elements. *Am. J. Phys. Anthropol.* **117**, 169 (2002). doi:10.1002/ajpa.20017 Medline

42. R. Kidd, C. Oxnard, Little Foot and big thoughts—a re-evaluation of the Stw573 foot from Sterkfontein, South Africa. *HOMO J. Comp. Hum. Biol.* **55**, 189 (2005). doi:10.1016/j.jchb.2004.07.003

43. R. A. Reyment, R. E. Blackwith, N. A. Campell, *Multivariate Morphometrics* (Academic Press, London, 1984).

44. G. H. Albrecht, Multivariate analysis and the study of form, with special reference to canonical variates analysis. *Am. Zool.* **20**, 679 (1980).

45. G. H. Albrecht, Assessing the affinities of fossils using canonical variates and generalized distances. *Hum. Evol.* **7**, 49 (1992). doi:10.1007/BF02436412

46. W. R. Atchley, C. T. Gaskins, D. Anderson, Statistical properties of ratios 1. Empirical results. *Syst. Zool.* **25**, 137 (1976). doi:10.2307/2412740

47. R. S. Corruccini, Multivariate analysis in biological anthropology: Some considerations. *J. Hum. Evol.* **4**, 1 (1975). doi:10.1016/0047-2484(75)90086-X

48. R. J. Smith, W. L. Jungers, Body mass in comparative primatology. *J. Hum. Evol.* **32**, 523 (1997). doi:10.1006/jhev.1996.0122 Medline

49. H. M. McHenry, Body size and proportions in early hominids. *Am. J. Phys. Anthropol.* **87**, 407 (1992). doi:10.1002/ajpa.1330870404 Medline

50. B. Latimer, J. C. Ohman, C. O. Lovejoy, Talocrural joint in African hominoids: Implications for *Australopithecus afarensis*. *Am. J. Phys. Anthropol.* **74**, 155 (1987). doi:10.1002/ajpa.1330740204 Medline

51. J. M. DeSilva, A. Papakyrikos, A case of valgus ankle in an early Pleistocene hominin. *Int. J. Osteoarchaeol.* 22 June 2010 (10.1002/oa.1185). doi:10.1002/oa.1185